Fuel 298 (2021) 120357

Contents lists available at ScienceDirect

Fuel

journal homepage: www.elsevier.com/locate/fuel

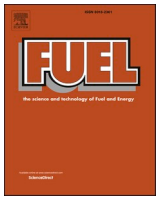

Full Length Article

An integrated geochemical, spectroscopic, and petrographic approach to examining the producibility of hydrocarbons from liquids-rich unconventional formations

Thomas Gentzis [a,*], Humberto Carvajal-Ortiz [a], Z. Harry Xie [a], Paul C. Hackley [b], Hallie Fowler [a]

[a] Core Laboratories L.P., Advanced Technology Center, 6316 Windfern Road, Houston, TX 77040, USA
[b] U.S. Geological Survey, MS 956 12201 Sunrise Valley Dr., Reston, VA 20192, USA

ARTICLE INFO

Keywords:
Hydrous pyrolysis
Multi-heating step pyrolysis
HF-NMR T1-T2 mapping
Organic petrography
Liquids-rich unconventional
Hydrocarbon producibility

ABSTRACT

The geochemical and petrophysical complexity of source-rock reservoirs in liquids-rich unconventional (LRU) plays necessitates the implementation of a more expansive analytical protocol for initial play assessment. In this study, original samples from selected source-rock reservoirs in the USA and the UK were analyzed by 22 MHz nuclear magnetic resonance (HF-NMR) T1-T2 mapping, followed by hydrous pyrolysis, and a modified Rock-Eval pyrolysis method (multi-heating step method-MHS). The above methods were complemented by organic petrography under reflected white and UV light excitation of the original and pyrolyzed samples. The analytical protocol presented attempts to better qualify and quantify different petroleum fractions (mobile, heavy hydrocarbons, viscous, solid bitumen), thus provide valuable and refined information about producibility of target intervals during appraisal. Results show how the hydrocarbon fractions interpreted from peak locations and intensities on NMR T1-T2 maps are in good agreement with those from MHS pyrolysis in terms of hydrocarbon mobility/producibility. Results from HP (Hydrous Pyrolysis) experiments show that an exception to this general agreement between NMR and MHS estimates occurs for the Kimmeridge Blackstone Clay samples, where MHS shows an increase of >90% in producible hydrocarbon yields vs. minimal to no presence of mobile hydrocarbons in NMR T1-T2 maps. This study clarifies the role of pore structure and networks in these discrepancies of producible oil estimates when comparing programmed pyrolysis to NMR-based techniques. This novel, multi-step and multidisciplinary approach provides a more advanced screening protocol for identifying zones of higher oil-in-place (OIP) and predicting fluid mobility prior to drilling or completions.

1. Introduction

Liquids-rich unconventional (LRU) plays are unconventional resource systems that contain large quantities of in-situ producible oil from the organic-rich shales themselves (indigenous) or from associated organic-lean, adjacent reservoir facies (exogenous; e.g., carbonates and siltstones; [1,2]. A full characterization of liquids-rich or shale-oil resources is no easy task due to their highly variable geochemical and petrophysical characteristics that make a liquid-rich resource producible. Among those characteristics, a proper initial assessment of the quantity of producible oil-in-place (OIP) is arguably one of the most important [1]. Current methodologies to evaluate OIP rely mostly on petrophysical modeling, charge models, and direct measurements on rocks analyzed in the lab, usually via open system programmed pyrolysis.

Open system programmed pyrolysis, commonly known as Rock-Eval pyrolysis [3] has been the industry's workhorse of source-rock screening for over 40 years. Although originally developed for source-rock evaluation of immature to marginally mature samples [4,5], customizing the pyrolysis program to best suit the geochemical and geological characteristics of particular hydrocarbon plays (e.g., shale-oil plays) is trivial in modern programmed pyrolysis instruments [6,7]. The need for customized pyrolysis programs is in response to the complex nature of LRU plays [7,8]. Despite the availability for over 20 years of customizable pyrolysis programs that would yield better characterization results [6,9], most analytical protocols for geochemical screening and assessment of LRU plays rely heavily on the analysis of as-received and solvent-extracted powdered material, using a single pyrolysis program

* Corresponding author.
E-mail address: thomas.gentzis@corelab.com (T. Gentzis).

https://doi.org/10.1016/j.fuel.2021.120357
Received 10 December 2020; Received in revised form 26 January 2021; Accepted 28 January 2021

(initial isotherm at 300 °C for 3–5 min, followed by a ramp of 25 °C/min to 550 °C° or 650 °C, depending on the instrument used), regardless of the nature of the LRU play [10–13]. The greatest challenge this analytical methodology faces is the uncertainty in determining how much of the extractable bitumen can be truly considered as part of the OIP, and thus contribute to hydrocarbon producibility.

Only a few recent well-documented studies have included modified pyrolysis programs in the evaluation of LRU plays. For instance, Romero-Sarmiento et al. [14] presented an example of the advantages of such customized pyrolysis programs, where modified pyrolysis methods, jointly with Thermal Extraction-Gas Chromatography (TE-GC), showed an improved understanding of geochemical properties of the Doig Formation in Canada as a LRU play. Similarly, Abrams et al. [8] proposed a non-pyrolysis high-resolution thermal extraction methodology (referred to as MiSTE) to better map out zones of high OIP that could indicate zones having a higher likelihood of containing producible liquid hydrocarbons. Recently, a low-temperature hydrous pyrolysis (LTHP) approach (heating a crushed mature source-rock core sample isothermally at 300 °C for up to 72 h) has been proposed by Nowaczewski et al. [15] as a way to determine the quality and quantities of retained oil in tight oil reservoirs. Results have been encouraging, including the ability to measure the API (American Petroleum Institute) value of the oil and obtain its Gas Chromatography (GC) and Gas Chromatography-Mass Spectrometry (GC–MS) signatures. However, the authors stated that the LTHP is not a substitute to Rock-Eval pyrolysis but a complimentary analysis.

The complexity of organic-rich source-rock reservoirs in LRU plays requires the implementation of alternative techniques for initial play assessment, in addition to pyrolysis-based methods. One such alternative is nuclear magnetic resonance (NMR) relaxometry. Few studies have attempted to integrate geochemical screening techniques and hydrogen NMR for the assessment of LRU plays [16–20]. In one of the only peer-reviewed studies on the use of modified, multi-heating step (MHS) programmed-pyrolysis methods in tandem with H-NMR, Romero-Sarmiento et al. [6] showed that NMR T1-T2 maps and the T1/T2 ratio can be used to distinguish bitumen, oil, and organic matter in the Vaca Muerta Formation, Argentina. Their study correlated TOC (Total Organic Carbon) obtained from a modified Rock-Eval pyrolysis method (the IFPen Shale Play® method) to 'solid echo' signal intensities calculated by hydrogen NMR T1-T2 mapping. Similarly, Piedrahita and Aguilera [13] proposed a model to estimate the Oil Saturation Index, OSI (S1 × 100/TOC) from NMR TOC logs and back-calculate S1 (and OIP) for evaluation of producible oil in shale plays.

When dealing with unconventional formations, such as shale oil or shale gas, with low porosities, nanoscale pore sizes, co-existence of water, and ultra low permeabilities, the traditional low frequency (LF, ~2 MHz) NMR is insensitive and unable to detect fast decay signals from solid organic matter or is lacking the resolution in T1-T2 maps to distinguish between water and oil. Since it was first introduced commercially in 2013, higher frequency (HF, at 22 MHz) NMR relaxometry techniques have quickly gained attention and acceptance in unconventional core analysis as a means to obtain quality petrophysical properties. HF-NMR has the advantage of a 30–50-fold greater sensitivity than LF-NMR and much shorter inter-echo spacing time. As a result, the HF-NMR is an ideal tool to characterize unconventional mudstones because of its capability to detect hydrogen signals that come not only from water and oil but also from solid organic matter. The two-dimensional NMR mapping techniques [21] have gained attention because of their advantage in plotting T1 and T2 simultaneously. A main challenge in H-NMR and geochemical screening studies is to better define the cut-offs (both in T1-T2 mapping and pyrolysis parameters) for producible OIP.

Hydrous pyrolysis (HP) is a well-known artificial maturation technique and has been used to study the optical texture changes of organic matter in source rocks and the kinetic behavior of different types of organic matter [22–24]. Although HP has been widely used through the years for basin modelling and source-rock kinetics studies, we are not aware of any published studies that compare and contrast all three methods (HF-NMR, MHS, HP) in the context of producibility for samples from LRU plays.

The main objectives of this multidisciplinary study are to: a) determine whether the changes seen optically in the HP residues are detectable by MHS Rock-Eval pyrolysis and HF-NMR T1-T2 mapping; and b) investigate whether there is a correlation between MHS pyrolysis results and HF-NMR data (for solid and liquid organic phases), particularly when NMR measurements are made above room temperature (22 °C), thus refining the estimates of mobile and producible hydrocarbons under reservoir conditions. The proposed analytical protocol provides improved and complementary estimates of the hydrocarbons that are likely to be produced.

2. Analytical methods

2.1. Sample selection

Samples were selected from thermally immature outcrops of the Upper Jurassic Kimmeridge Clay Formation in the UK and the Green River Shale Formation in the USA. The Kimmeridge Clay sample, labeled KC-Original, was collected from an outcrop in the type area on the Dorset coast of England. The sample labeled APM-Original is a laminated lacustrine oil shale from the informal Mahogany zone of the Eocene Green River Formation. The sample was collected from an outcrop at the Anvil Points Mine, Piceance Basin, Colorado. Since the samples were collected at outcrop, there is a possibility of weathering. However, the samples were selected by sledging back into the outcrop to reduce the likelihood of weathering. In the case of the APM-Original sample, a portable hole drill was used to core into the Mahogany Zone. Furthermore, no weathering effects were detected under the microscope and the original samples had low Oxygen Index (OI) values, which indicates that weathering has not occurred. For additional information on the mineralogy and organic matter (kerogen) properties of the two original samples, the reader is referred to Birdwell and Washburn [17,18] and Washburn et al. [25].

Both formations exhibit excellent organic-richness and oil-proneness, but also contrasting organic matter type properties and thermal evolution characteristics. For example, the lacustrine organic matter in the APM-Original sample does not enter the threshold for hydrocarbon generation until vitrinite reflectance (Ro) values of ~0.90%. On the other hand, the marine organic matter in sample KC-Original enters the oil window at Ro values of ~0.60%. These characteristics make an excellent substrate matter for experiments on thermal maturation and hydrocarbon quantification.

2.2. Multi-heating step (MHS) pyrolysis

About 60 mg of crushed rock chips were analyzed using a Rock-Eval 6® Turbo analyzer and 90 mg of crushed samples using a Rock-Eval 7S® analyzer (Vinci Technologies, France). The Rock-Eval 7S® was used because of its sulfur detection capabilities and ability to directly quantify the total organic sulfur (TOS) in whole-rock and kerogen concentrate samples. The amount of organic sulfur in sedimentary organic matter (quantified as TOS) is a critical parameter that directly influences source-rock kinetics and thus, thermal conversion of organic matter into hydrocarbons. Our MHS pyrolysis program was similar to the one described by Abrams et al. [8], with minor modifications. Briefly, the pyrolysis oven program started at a temperature of 80 °C and immediately ramped to 200 °C at a rate of 50 °C/minute and maintained isothermal for 15 min. The second ramp was to 250 °C with 50 °C/minute and maintained isothermal for 15 min. The third ramp was with 50 °C/minute to 300 °C and maintained isothermal for 15 min, followed by a fourth ramp of 50 °C/minute to 350 °C and maintained isothermal for 15 min. The fifth and last ramp was to 650 °C at 25 °C/minute. The

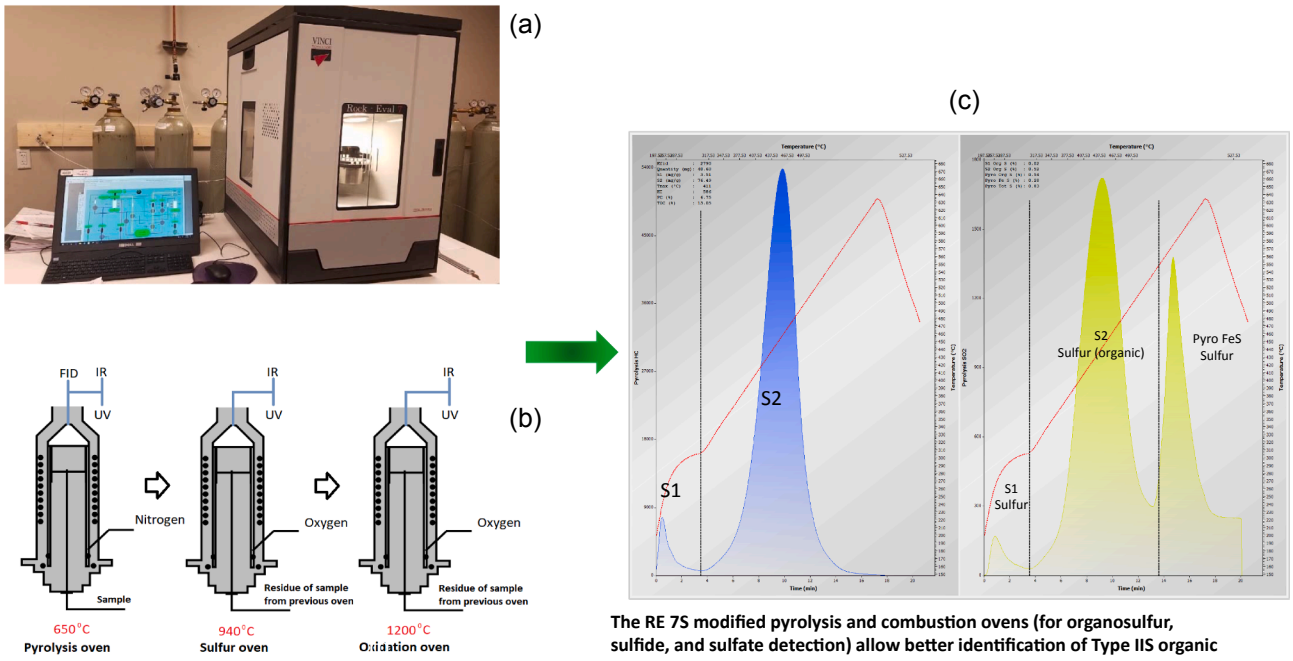

Fig. 1. Photograph of the Rock-Eval 7S instrument (a) showing schematic diagram of the pyrolysis and combustion ovens (b) and pyrograms of the sulfur species (c).

sulfur speciation analysis was performed using the Basic/Total Sulfur method (IFP methods). The temperature program is similar to the Basic/Bulk-Rock method widely used in the industry (pyrolysis isothermal at 300 °C for 3 min, followed by a 25 °C/minute ramp until 650 °C), but with an extended analysis time during the oxidation stage (with a 20 °C/minute ramp from 300 °C to 1200 °C for full decomposition of sulfate moieties). More details of the sulfur speciation using Rock-Eval 7S instrumentation can be found in Lamoureux-Var et al. [26], Aboussou et al. [27] and Wattripont et al. [28]. Fig. 1 shows a schematic of the instrumentation.

2.3. Hydrous pyrolysis

Samples examined herein were subjected to HP experiments. A complete description of the hydrous pyrolysis method with SwageLok™ mini reactors was recently provided by Hackley and Lewan [24]. 23 Crushed rock chips (2–4 g, 1–3 mm top size) were loaded into SwageLok™ mini-reactor vessels (25–35 mL internal volumes). The rock chips were covered with deionized water and the reactor was placed in a gas chromatograph oven at the selected temperatures (300 °C, 320 °C, 330 °C, 340 °C, 350 °C, 360 °C) for 72 h. Solid rock residue from each experiment was collected for MHS pyrolysis, hydrogen NMR measurements, and organic petrography analysis.

2.4. HF-NMR T1-T2 mapping

Hydrogen-NMR relaxometry measurements were made at Core Laboratories with a special 22 MHz spectrometer from MR Cores, equipped with a 30 mm diameter probe. The NMR probe size allowed for measurements on samples of any shape or form that can be loaded into sample vials. The T2 data were acquired using the Carr-Purcell-MG (CPMG) sequence with an echo time spacing of 0.07 ms. The T1 data were acquired using an inversion-recovery sequence. The T1-T2 correlation data were acquired using a pulse sequence of combining T1 and T2 data acquisitions, where the amplitude was determined from the first echo, then processed using an Optimized Truncated Singular Value Decomposition (OTSVD) inversion method to obtain the 2D T1-T2 map. All analyses were performed at room temperature of 22 °C unless otherwise noted. The NMR instrument was calibrated against a known weight or volume of liquid sample, usually doped water sample, that was provided by the instrument vendor. The measured NMR signals of the samples were converted to the unit of mg based on the calibration.

2.5. Organic petrography

Detailed sample preparation and analysis procedures are described in [29–31]. Briefly, whole-rock (WR) samples were crushed to 20 mesh (850 μm or 0.85 mm size) particles. Ground particles were placed in specially designed plastic molds (1.5 in. or 3.8 cm in diameter) where they were mixed with epoxy resin and hardener (ratio of 2:1) to harden overnight. Sample grinding and polishing was performed using Buehler EcoMet/AutoMet 250 automated polishing equipment. Reflectance in oil (Ro) and fluorescence analyses were performed using a Carl Zeiss Axio Imager A2m microscope, equipped with a white halogen light source (from a 12 V/100 W halogen lamp with stabilized current) and a UV light (fluorescence) source (from a high pressure 100 W mercury lamp with stabilized current) which allows for observation of the fluorescence colors of oil-prone organic matter (OM) (alginite, sporinite, dinoflagellates, etc.) when in the oil window. A sapphire standard (0.595 %Ro) was used for the reflectance analysis.

2.6. Argon ion milled-scanning electron microscopy (AIM-SEM)

A representative portion of the two original samples was polished with a Leica EM TIC3x argon ion mill in order to create a flat, artifact-free surface suitable for analysis with backscattered electrons. To document the characteristics of the sample with backscattered electrons, secondary electron, and/or backscattered electron images with superimposed secondary electron images were taken using a FEI Quanta FEG250 Scanning Electron Microscope operating at relatively low beam energy (10 kV–15 kV) in a high pressure (~60 Pa or 0.09 psi) vacuum chamber environment. Using relatively low beam-energy and high-pressure chamber environment mode helps to avoid the evaporation of any volatiles that may be associated with the organic matter. A benefit of backscattered electron imaging is that it is easier to identify specific mineral grains. This is because the various 'grey-levels' of the image are

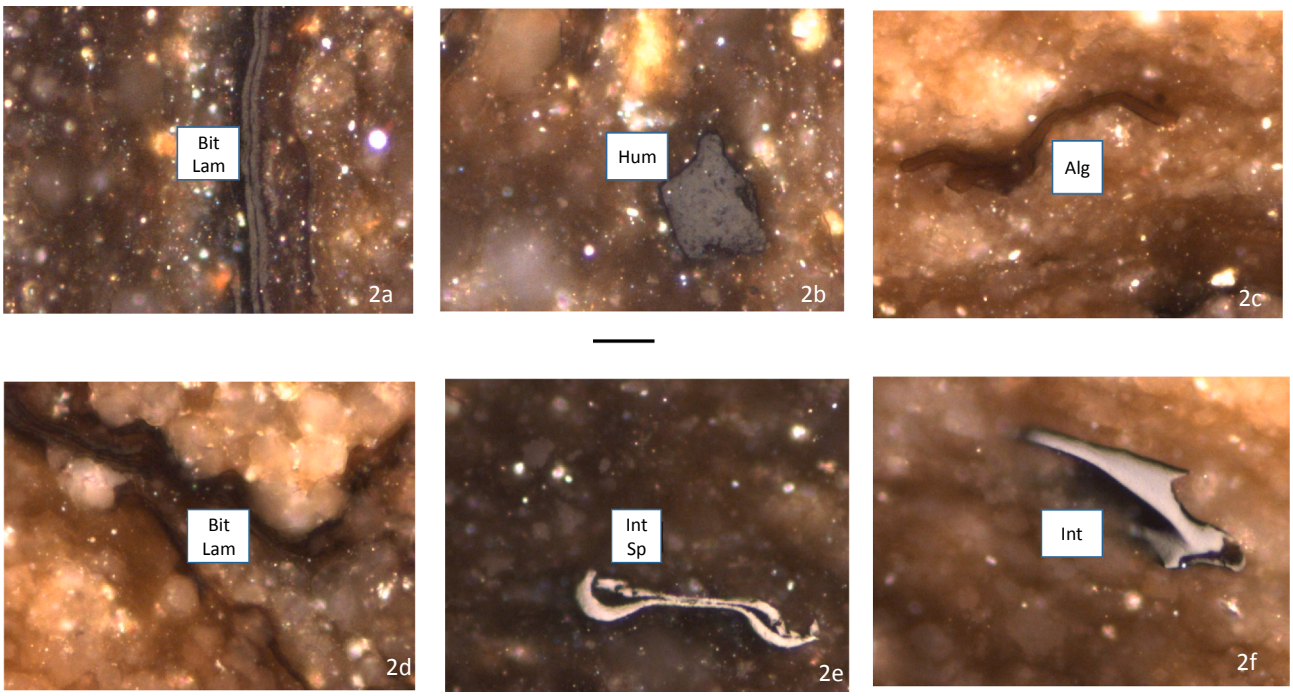

Fig. 2. Microphotographs of original AMP-Original sample: Thin (<5 μm) bitumen lamellae (a); Huminite (b); Telalginite (c); Bitumen lamellae (d); Inertinized sporinite (e); Inertinite (f). The scale bar has a length of 10 μm.

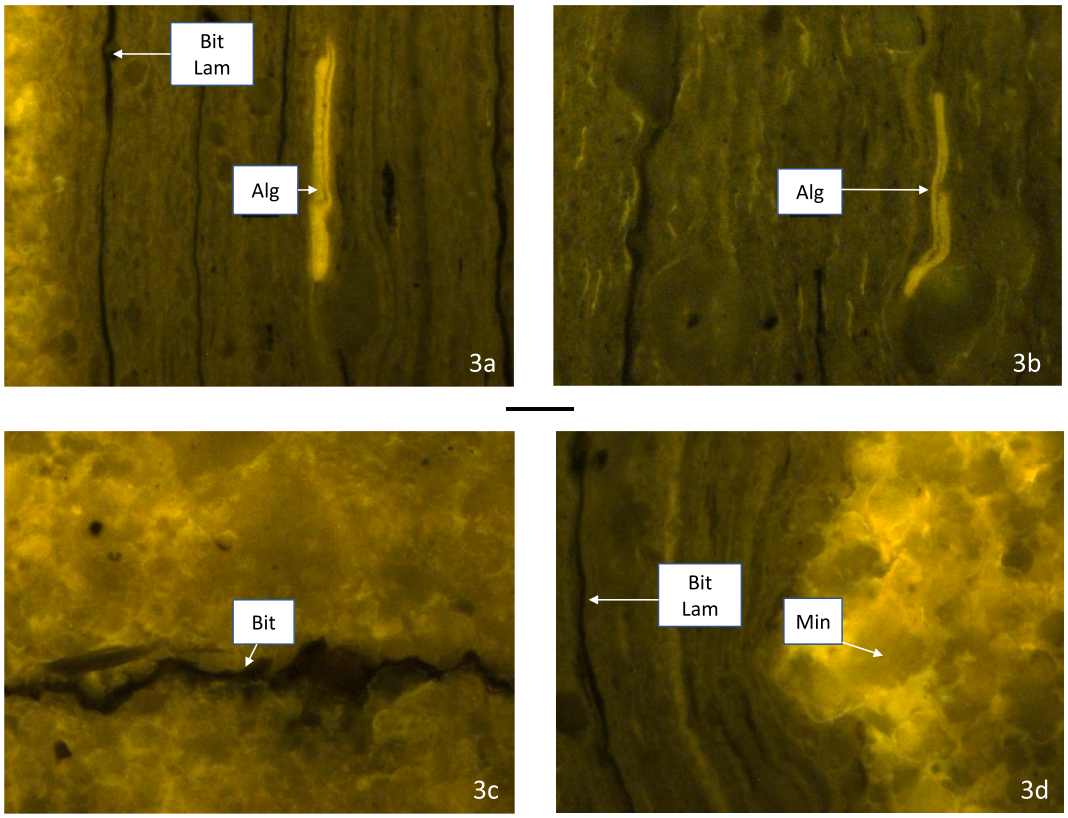

Fig. 3. Telalginite, bitumen lamellae and fluorescing amorphous matrix (a); telalginite, liptodetrinite and fluorescing amorphous matrix (b); bitumen in fracture (c); bitumen lamella, fluorescing matrix and minerals (d). Scale bar is the same as in Fig. 2. UV light excitation is at 465 nm; combined dichroic and barrier filter has a cut at 510 nm.

a function of the density of the minerals; higher density minerals are white (e.g., pyrite) and the lowest density grains (e.g., organic matter) are black.

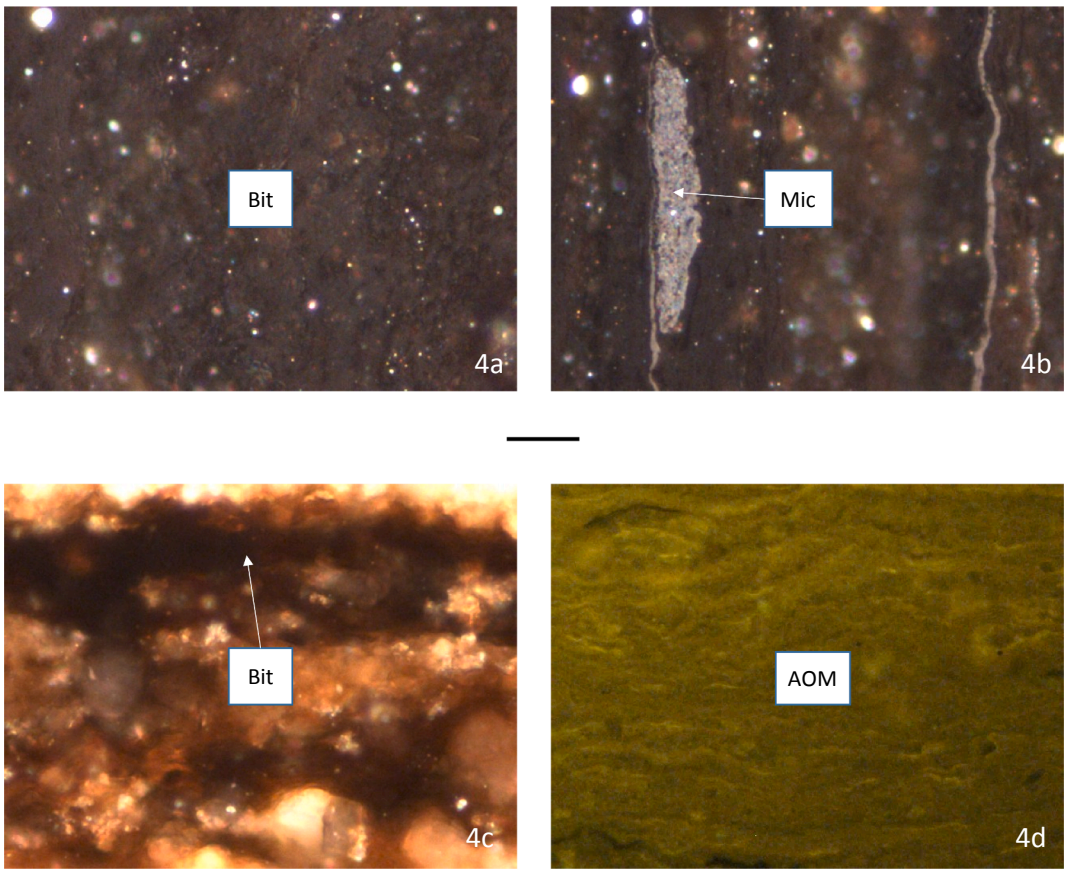

Fig. 4. Microphotographs of APM HP residue at 300 °C: Dark-grey non-native matrix bitumen (%Ro = 0.10) (a); thin bitumen lamella bright-grey micrinite (%Ro = 0.35) (b); bitumen (Bit) deposited between minerals (c); fluorescing amorphous organic matrix (AOM) (d). Scale bar is the same as in Fig. 2.

3. Results and discussion

3.1. Organic petrography of the APM-original sample

Lacustrine oil shales, including the Green River Shale, are often rich in Type I kerogen, which is distinguished by its very high organic hydrogen content (kerogen H/C ratios >1.2). Sample APM-Original was deposited in a lacustrine environment [32], thus the algal organic matter is interpreted to represent deposition and preservation as benthic microbial mats [33]. Type I kerogen is abundant in the APM-Original immature sample and occurs primarily as strongly fluorescing amorphous and laminated organic matter (AOM) and liptodetrinite. Native solid bitumen and rare vitrinite-like particles are also present. Representative microphotographs under reflected white light are shown in Fig. 2. Fig. 2a shows native solid bitumen in the form of elongate and thin (5–10 μm) lamellae that occur parallel to bedding, as also reported by [24]. Fig. 2b shows a huminite-like (precursor of vitrinite) particle having low reflectance (%Ro is 0.25). Oil-prone unicellular telalginite is seen in Fig. 2c and solid bitumen lamellae in Fig. 2d. Sample APM-Original also contains inertinized sporinite (Fig. 2e) and inertinite (Fig. 2f). Under reflected UV light excitation, the AOM has greenish-yellow fluorescence color and telalginite exhibits golden-yellow fluorescence (Fig. 3a, b). Solid bitumen lamellae do not fluoresce (Fig. 3c, d).

3.1.1. APM HP residues

Representative microphotographs of the 300 °C residue are shown in Fig. 4. Fig. 4a shows newly formed (non-native) solid bitumen (dark grey areas) having %Ro of ~0.10 and Fig. 4b shows thin (<5 μm bitumen lamella) as well as bright-grey, granular, micrinite-like oval particles with %Ro of 0.35. The dark solid bitumen has replaced, in situ, the amorphous organic matter seen in the original sample. Orange-colored solid bitumen is seen deposited around the quartz grains (Fig. 4c). Under UV light, the thinly laminated amorphous organic matrix exhibits a weak fluorescence (Fig. 4d).

In the 320 °C residue, the newly generated solid bitumen has migrated to rock fragment edges and formed larger accumulations within the fragments (Fig. 5a). These textures indicate mobility of the petroleum phase. The reflecting surface is more homogeneous, suggesting mixing and homogenization of the petroleum components. Reflectance % is 0.18 in the 320 °C residue, indicating increased aromaticity. In the 330 °C residue, newly generated solid bitumen is more abundant than in the 320 °C residue, and its reflectance decreased but only slightly to 0.12%. Solid bitumen has migrated to grain boundaries and formed larger accumulations within residue fragments (Fig. 5b). In the 350 °C and 360 °C residues, solid bitumen is progressively less abundant. At 350 °C, solid bitumen has developed a coked texture with appearance of mesophase micro-domains with higher reflectance (Fig. 5c). These mesophase domains qualitatively increase in abundance from the 350 °C to 360 °C residues. Reflectance % of anisotropic coke domains of medium size mosaic at 360 °C (Fig. 5d) ranges from 1.50 to 1.66.

3.1.2. Organic petrography of the KC-Original sample

Previous workers have provided detailed descriptions of organic petrography and mudstone lithofacies of the Kimmeridge Clay Formation [34–38]. Representative microphotographs are shown in Figs. 6 and 7. The original immature sample contains native solid bitumen (Fig. 6a-b) and amorphous bituminite matrix, occasionally having a reddish-orange tint (Fig. 6c). Native solid bitumen has %Ro ranging from 0.25 to 0.32 (mean is 0.28%). Vitrinite-like particles (Fig. 6d) are rare and have %Ro of 0.52–0.57 (mean is 0.53%). Other macerals present include faunal inertinite (Fig. 6e) and inertinite (Fig. 6f). Granular micrinite is

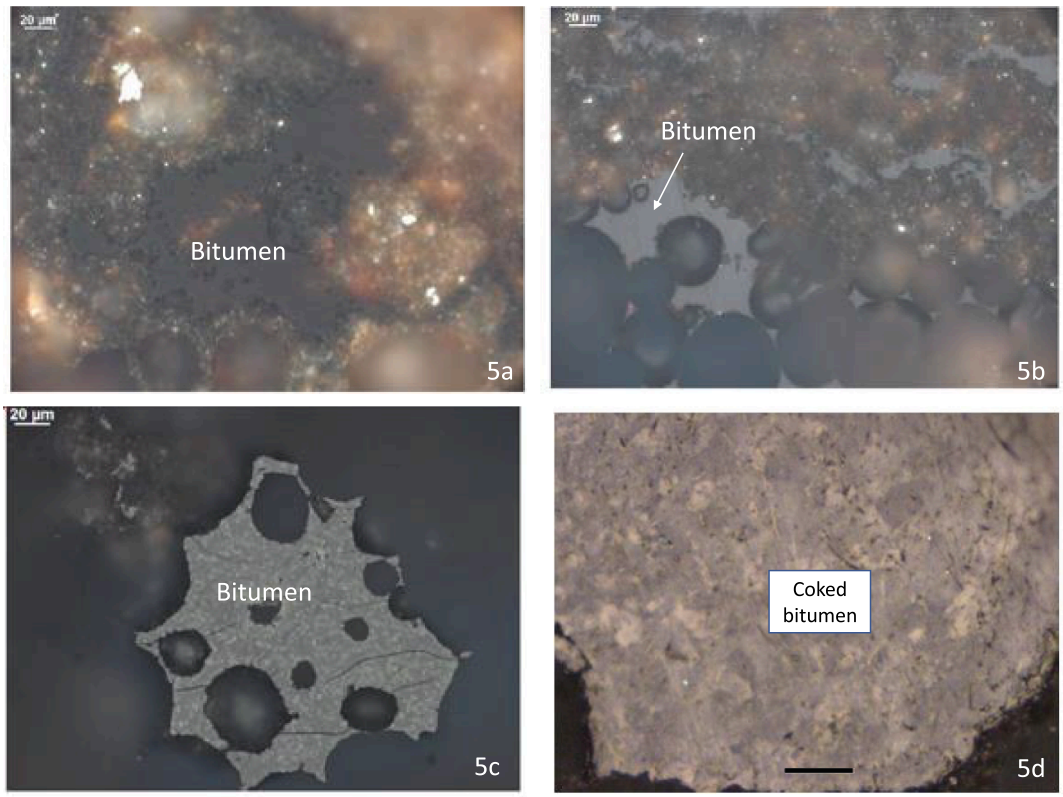

Fig. 5. Microphotographs of APM HP residues: bitumen at 320 °C (a); angular bitumen at 340 °C (b); vacuolated bitumen with mosaic texture at 350 °C (c); coked bitumen with medium-grained mosaic texture (d). Scale bar in Fig. 5d is 10 µm.

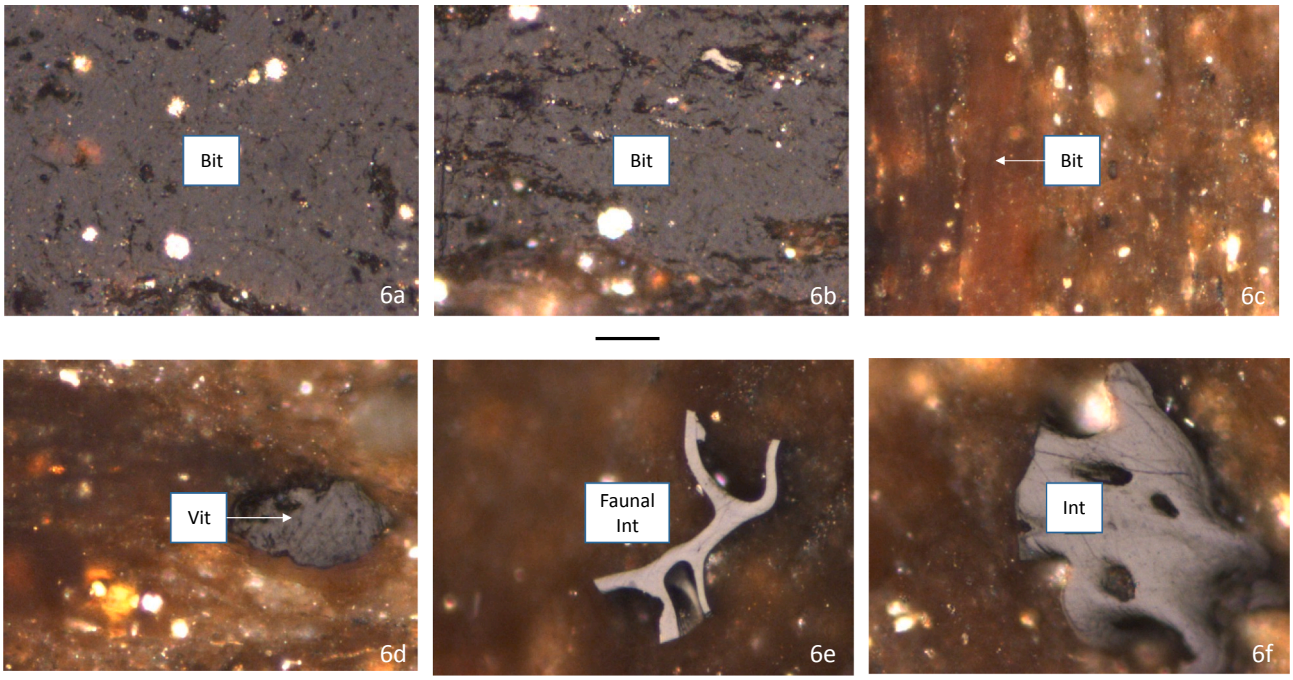

Fig. 6. Microphotographs of original KC-Original sample: Non-native solid bitumen (a-b); orange-colored bitumen (c); vitrinite-like particle (d); Faunal inertinite (e); inertinite (f). Scale bar is the same as in Fig. 2. (For interpretation of the references to color in this figure legend, the reader is referred to the web version of this article.)

rare and is the result of the early conversion of AOM to hydrocarbons. Excitation under UV shows the presence of strongly-fluorescing (with golden-yellow color) marine telalginite encountered normal to bedding (Fig. 7a-b) and parallel to bedding (Fig. 7c). Amorphous fluorescing matrix is present throughout having a weak dull-yellow fluorescence (Fig. 7d). Fossilized fish bones have been replaced by sulfides. Radiation damage halos are present in the form of zones of reduced fluorescence intensity surrounding heavy minerals that are included in AOM.

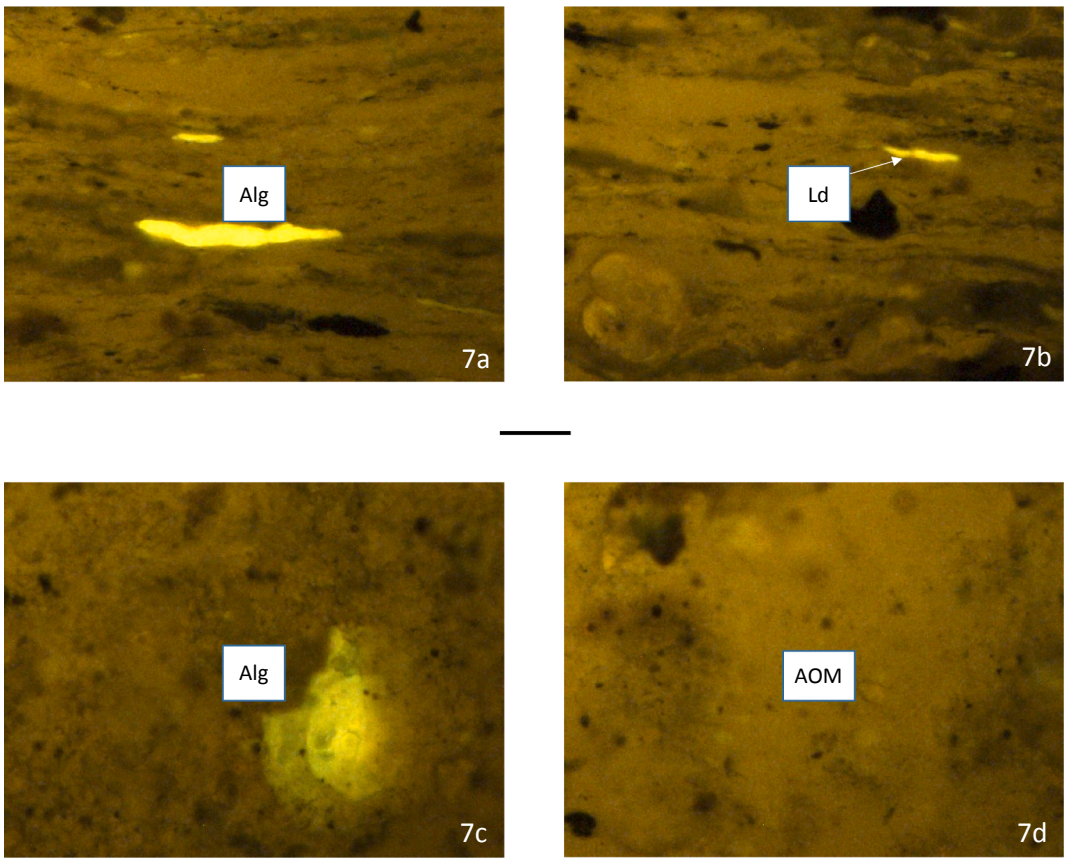

Fig. 7. Golden-yellow fluorescing telalginite and weakly-fluorescing amorphous organic matrix (a); fluorescing amorphous organic matrix and telalginite (b); telalginite parallel to bedding (c); amorphous organic matter (AOM) having dull-yellow fluorescence (d). Scale bar is the same as in Fig. 2. (For interpretation of the references to color in this figure legend, the reader is referred to the web version of this article.)

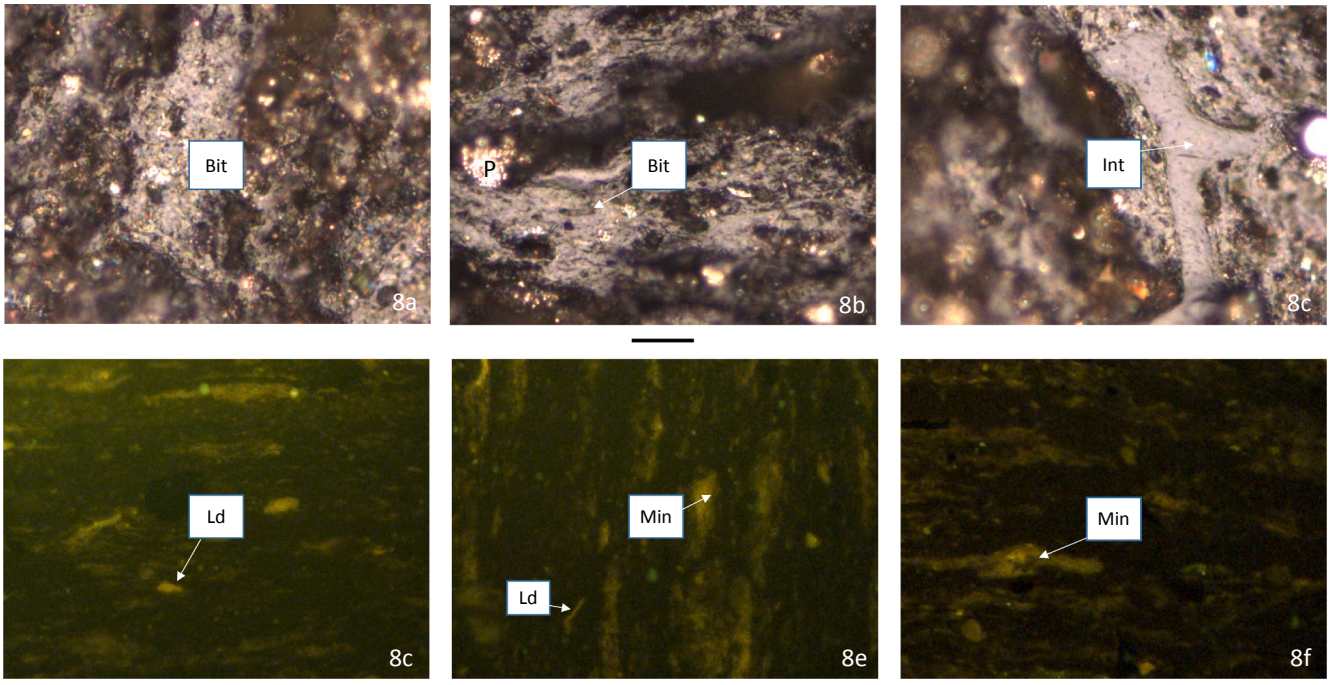

Fig. 8. Microphotographs of KC HP residue at 300 °C: Bitumen (a-b) (%Ro = 0.35); inertinite (c); fluorescing liptodetrinite, mineral matter and amorphous matrix (d-f). Scale bar is the same as in Fig. 2.

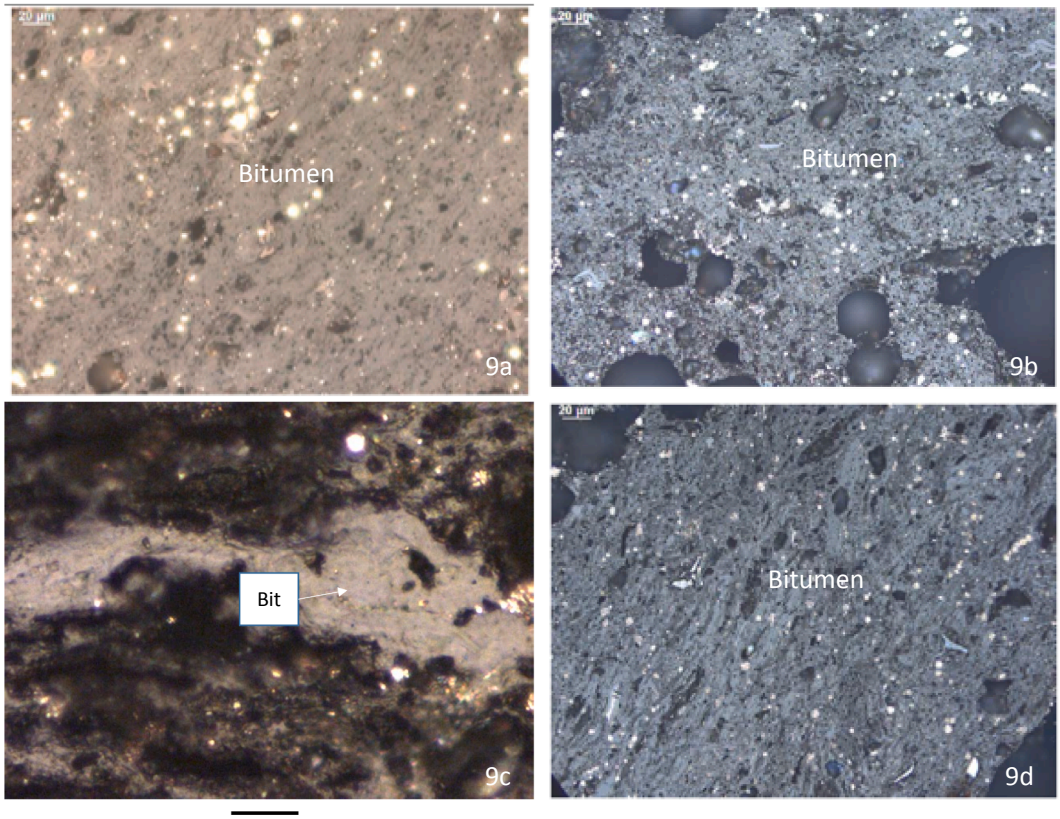

Fig. 9. Microphotographs of KC HP residues: Bitumen at 340 °C (a); bitumen at 360 °C (b); also, bitumen at 360 °C (c); bitumen at 370 °C (d). Scale bar in Fig. 9c is 10 μm.

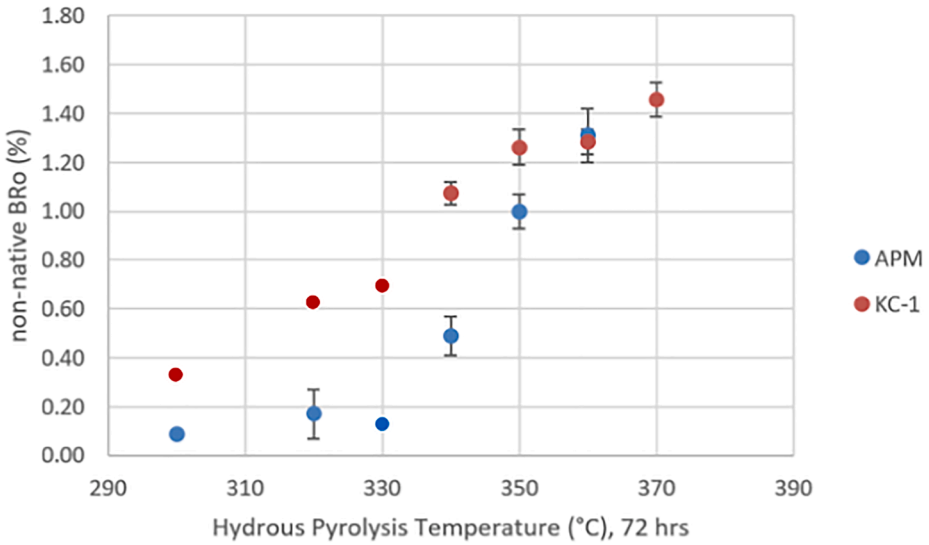

Fig. 10. Relationship between HP temperatures vs. non-native bitumen %Ro for the original samples and their HP residues.

3.1.3. KC HP residues

Representative microphotographs of the 300 °C residue are shown in Fig. 8. A continuous matrix of solid bitumen is present with entrained clay mineral matter (Fig. 8a), pyrite framboids (Fig. 8b), and inertinite (Fig. 8c). Solid bitumen reflectance (%Bro) ranges from 0.30 to 0.36. UV light shows the presence of weakly-fluorescing mineral particles (Fig. 8d–f). The bitumen %Ro is 0.62 in the 330 °C residue. In the 340 °C residue, a continuous matrix of solid bitumen is present with entrained mineral matter and refractory terrestrial kerogen (Fig. 9a). The 360 °C residue contains vacuolated bitumen matrix enclosing pyrite (Fig. 9b) and layers of solid bitumen having high reflectance (%Ro 1.3–1.5) (Fig. 9c). Although the solid bitumen in residues at 350 °C and 360 °C (Fig. 9d) is progressively higher in reflectance, qualitatively it has a similar texture and is approximately constant in abundance.

The observation that solid bitumen abundance is constant in the KC HP residues contrasts to that in the HP residues of sample APM, in which solid bitumen is visually estimated to be progressively less abundant at higher HP temperatures. The higher expulsion efficiency in APM compared to KC could be explained by compositional differences of the newly generated solid bitumen in response to thermal stress. Solid

Table 1
Basic/Bulk-Rock, Multiple Heating Step (MHS) pyrolysis and high frequency-nuclear magnetic resonance (HF-NMR) data of the original samples APM-Original and KC-Original and their HP residues at 300 °C, 330 °C, and 360 °C.

Sample ID	Method	L1	L2	L3	L4	OIL (S1, Σ L1-L4 or Σ NMR 2–5)	S2	S2-Ext.
KC-1	BASIC					3.34	262.32	212.71
	MHS	2.37	3.21	5.88	29.74	41.2	228.88	
	NMR					24.56	235.1	
KC-300	BASIC					39.71	248.24	36.01
	MHS	26.1	20.08	20.69	23.19	90.06	198.49	
	NMR					34.85	190.2	
KC-330	BASIC					48.01	175.86	21.32
	MHS	32.52	31.72	29.32	27.48	121.04	109.51	
	NMR					44.55	141.9	
KC-360	BASIC					68.43	87.52	15.32
	MHS	47.88	33.35	21.91	13.97	117.11	34.67	
	NMR					92.58	59	
APM-1	BASIC					5.42	192.82	180.72
	MHS	2.93	2.43	3.59	8.55	17.5	182.94	
	NMR					16.32	187.5	
APM-300	BASIC					9.29	159.5	110
	MHS	5.46	6.67	7.33	8.17	27.63	144.14	
	NMR					31.89	154.6	
APM-330	BASIC					16.38	121.62	26.14
	MHS	8.56	11.49	11.84	11.88	43.77	99.73	
	NMR					49.7	103.4	
APM-360	BASIC					12.5	25.31	6.7
	MHS	6.84	5.07	4.25	4.05	20.21	16.45	
	NMR					12.89	51.6	

bitumen in the KC HP residues may contain less aliphatic components whereas the solid bitumen in the APM residues may contain more aliphatic components, which interfere with aromatic sheet alignment. This would be consistent with the lacustrine kerogen Type I in APM-Original sample having higher HI (871 mg HC/g TOC) than the marine kerogen Type II in the KC-Original sample that has HI of 737 mg HC/g TOC.

The measured BR_o values show significant differences between non-native, newly generated solid bitumen in the APM and KC HP residues (Fig. 10). While the %Ro of the solid bitumen in the KC HP residues increases at an almost constant rate from 300 to 370 °C, the solid bitumen %Ro in the APM HP residues initially decreases slightly between 300 and 330 °C before increasing with temperature. The different rate at which the Ro of the solid bitumen increases with HP temperature is related to kerogen kinetics. The trend shows that lacustrine kerogen Type I shows a delay under artificial maturation conditions compared to marine kerogen Type II (non S-rich), in agreement with previous studies [4,39]. Espitalie et al. [4] placed the threshold to the oil window for Kimmeridge Shale Type II, low-sulfur kerogen at 430–435 °C whereas the Green River oil shale Type I kerogen has a threshold of 440–450 °C [39]. However, the KC-Original sample in this study is rich not only in total sulfur (5.38 wt%) but also in organic sulfur (4.96 wt%), as will be shown in the next section. As a result, the threshold to the oil window is expected to be lowered considerably for this Type II-S marine kerogen. Kinetics data (not included) showed that, at 450 °C the transformation ratio (TR) of KC-Original was 50% whereas the TR of the APM-Original was only 20%. The activation energy (Ea) of APM-Original was unimodal and peaked at 53 kcal/mol whereas the Ea of KC-Original was bell-shaped with a wider range and a peak at 51 kcal/mol. With increasing temperature, the trends of measured %Ro of the solid bitumen in both HP residues converge, and at 360 °C the Ro of solid bitumen from both samples is almost identical (Fig. 10). It is worth noting that the highest increase (jump) in %Ro occurs between 330 and 350 °C but is more pronounced for the APM set of samples. The above behavior has an implication on when kerogen enters the oil window and how the transformation ratio to hydrocarbons changes with increased maturation.

Similar to differences in reflectance reported for vitrinite in coal and native solid bitumen in shale in hydrous pyrolysis residues [24], the present study indicates significant compositional differences in the newly generated solid bitumen. The most important difference is the fact that the newly generated solid bitumen in the APM HP residues formed mesophase and mosaic coke whereas the solid bitumen in the KC HP residues did not. This suggests that the solid bitumen in APM is of the graphitizing type and that the solid bitumen in KC is non-graphitizing. Graphitizing carbons go through a fluid stage (mesophase liquid crystal) during pyrolysis (carbonization) prior to forming coke. The fluidity facilitates molecular mobility of the aromatic molecules, which results in the formation of lamellar molecules [40]. On the other hand, non-graphitizing carbons do not pass through a fluid stage and do not form mesophase and coke because cross-linking between the aromatic structural units prevents them from doing so [41].

3.2. Sulfur speciation and multiple heating step (MHS) pyrolysis

The total quantity of sulfur species (e.g., total sulfur-TS, total organic sulfur-TOS, and organic sulfur from labile kerogen, S2, and organic sulfur from oil/bitumen, S1) is listed in Table 1. Fig. 11 shows the pyrograms of the thermally immature KC-Original sample (a-b) and of the APM-Original sample (c-d) obtained by Rock-Eval 7S®. Fig. 12 shows the pyrograms of two analyses performed on sample KC-360 (from the HP experiment performed at 360 °C) using the same Rock-Eval 7S® instrument. The pyrogram in the upper panel (Fig. 12a) originates from the analysis performed using the Basic/Bulk-Rock pyrolysis method (initial isotherm at 300 °C for 3 min, followed by a ramp of 25 °C/min to 650 °C). The pyrogram in the lower panel (Fig. 12b) originates from the analysis performed using the modified pyrolysis method (MHS) as described in the Analytical methods section. From the values shown in Fig. 12(a-b) and in Table 1, it is evident that the Basic/Bulk-Rock method, which is commonly utilized in most play assessment projects, is not the appropriate or ideal analytical option when evaluating OIP in LRU plays because the Basic/Bulk-Rock pyrolysis method underestimated the S1 compared to the MHS pyrolysis method (68.4 vs 117.1 mg/g) regardless of the type of pyrolysis instrument used [6,7]. In other words, the sum of peaks L1-L4 from our MHS method (Fig. 12b) estimated the amount of non-kerogen hydrocarbons in the KC-Original

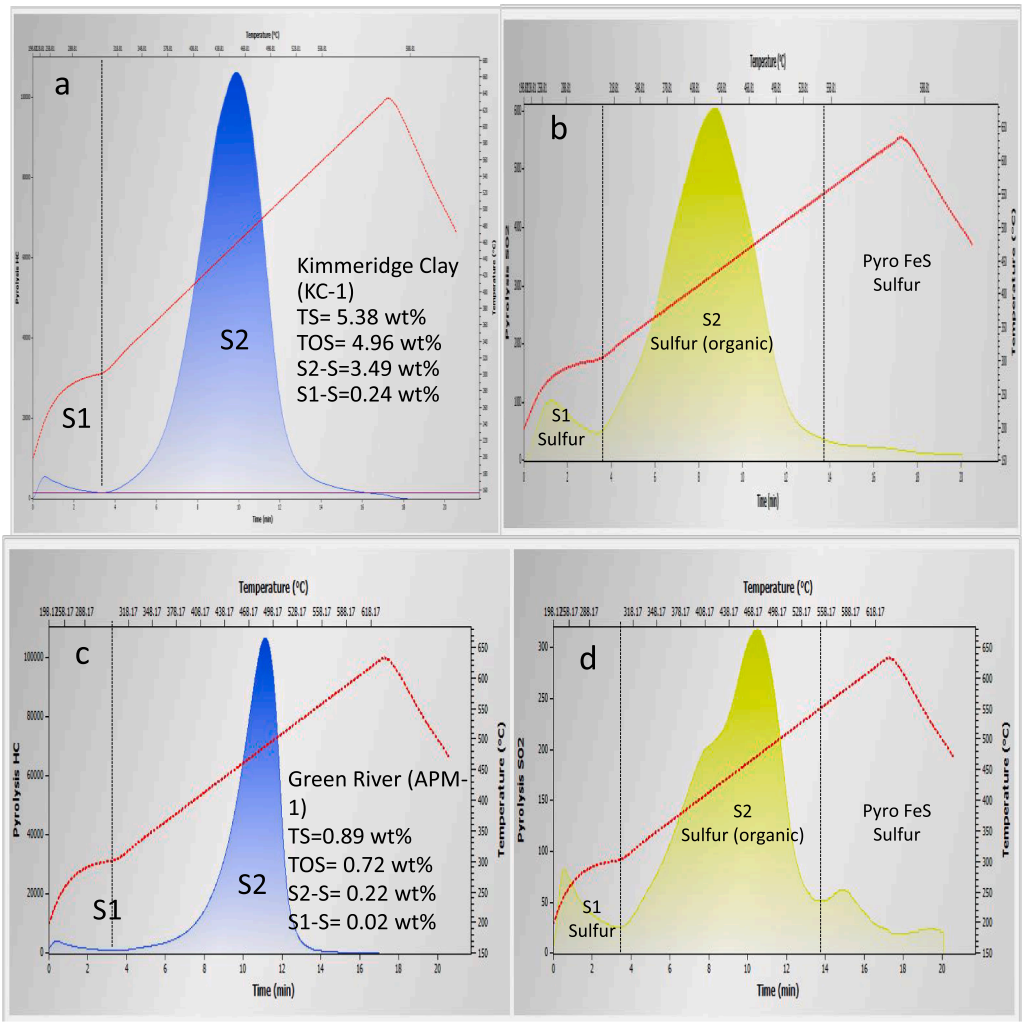

Fig. 11. (a–d) Sulfur quantities (total sulfur, TS, total organic sulfur, TOS, and organic sulfur from labile kerogen, S2, and oil/bitumen, S1) during pyrolysis of the thermally immature KC-Original (a-b) and APM-Original samples (c-d).

sample more closely than did the Basic/Bulk-Rock pyrolysis.

MHS pyrolysis results separate the free/adsorbed hydrocarbons (S1) present in LRU intervals into four (4) regions (labelled L1 through L4; Fig. 12b) corresponding to each of the isothermal steps of the MHS analysis. Region L1 (distilled at 200 °C) was interpreted by Carvajal-Ortiz et al. [42] to contain the lowest boiling-point (BP) hydrocarbons, as confirmed by Thermal Extraction-Gas Chromatography (low BP *n*-alkanes and aromatics). This observation is similar to the findings of Abrams et al. [7]. The hydrocarbons in each of the above four regions increase in complexity and their quantities could be used to evaluate their relative producibility. Thus, L1 is believed to represent hydrocarbons in intervals having the highest likelihood of being produced from the chemical composition point of view. Increasing molecular weight (heavier hydrocarbons and non-hydrocarbons) dominate the remaining free/adsorbed hydrocarbon regions in order of increasing distillation temperature (L2 < L3 < L4), thus reducing their likelihood of being produced. The MHS reflects the chemical composition (viscosity) of the hydrocarbons in each of the four regions but does not consider the petrophysical properties of the rock, such as its porosity and permeability.

An assumption has been made by numerous studies in the past that the "true" S1 = $(S1 + S2)_{\text{whole rock}} - S2_{\text{extracted}}$. In our opinion, this assumption is incorrect as the data in Table 1 shows. The sum of L1-L4 following MHS (column labelled "OIL", and which is equivalent to what the S1 represents in the Basic/Bulk-Rock method) is smaller than the sum of $(S1 + S2)_{\text{whole rock}} - S2_{\text{extracted}}$. For example, in sample KC-300 °C: $(S1 + S2)_{\text{whole rock}} = 39.71 + 248.24 = 287.95$ and $(S1 + S1)_{\text{whole rock}} - S2_{\text{extracted}} = 287.95–36.01 = 251.94$. The sum of L1-L4 from the MHS analysis for the same sample is 90.06, which is considerably lower. The same is true for samples KC-330 °C and KC-360 °C. This indicates that what is considered to be 'extractable' is not necessarily 'producible'. Based on TE-GC data (to be discussed in Section 3.5), we believe that only the hydrocarbons in regions L1, L2 and a fraction of region L3 will be 'producible'. The remaining of the L3 and all the L4 region hydrocarbons will not be considered to be 'producible' because these fractions contain heavy n-alkanes, resins, asphaltenes, and NSO compounds that will not flow and remain in the pores of the formation at depth. The exact percentage of hydrocarbons in region L3 that will be producible is not constant by will vary from one formation to another.

The large contrast in organic sulfur quantities between the two samples (in both TOS and S2-Sulfur) from Fig. 11 (a and c) has a direct implication on the amount (and quality) of hydrocarbons produced after each HP experiment (and also in naturally-occurring hydrocarbons generated from these two types of organic facies). Sulfur-carbon bonds are energetically more labile than carbon–carbon bonds; thus, oil-prone kerogen with higher quantities of organic sulfur (especially S2-bound sulfur) will generate hydrocarbons at lower levels of thermal stress than their sulfur-lean counterparts [39]. These "immature" hydrocarbons will inherently be richer in sulfur and will most likely be of lower quality (i.e., high sulfur content, higher viscosity and lower API gravity),

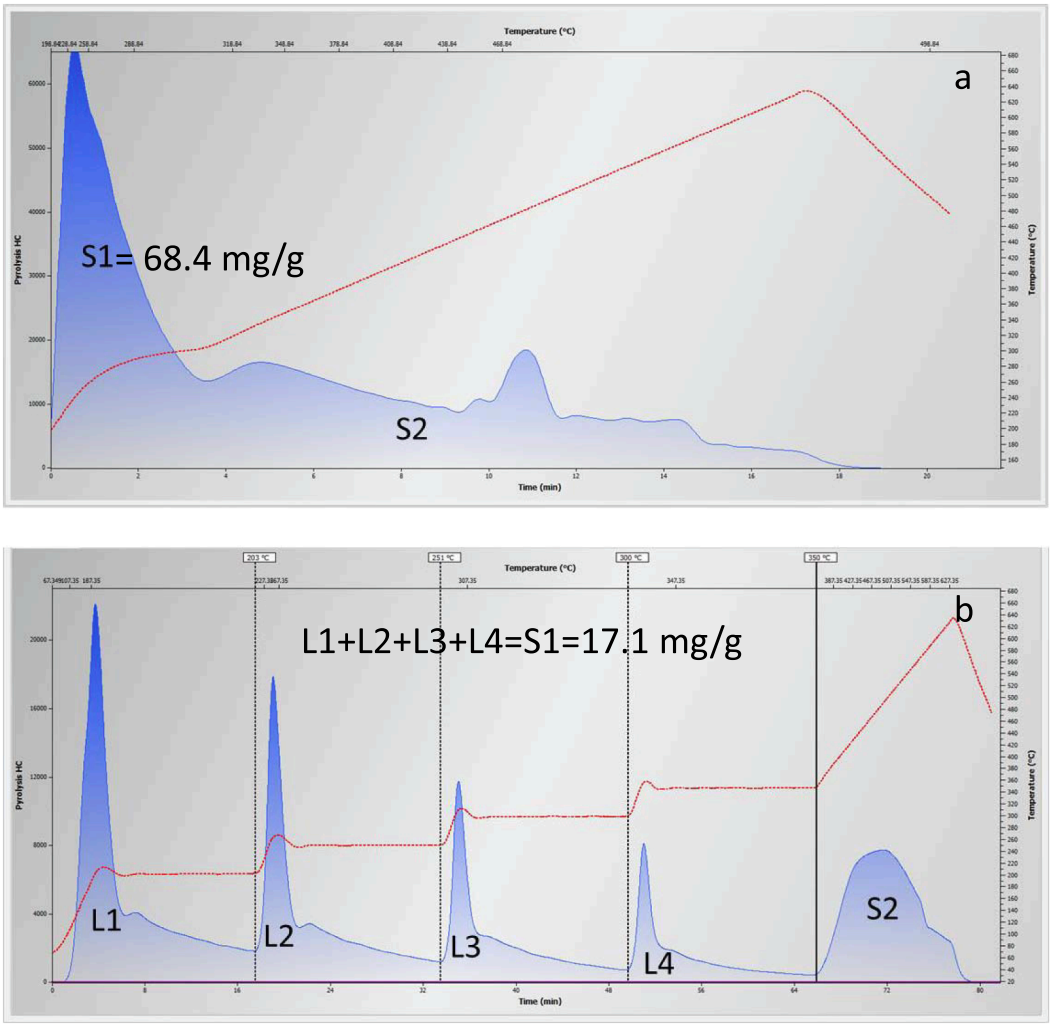

Fig. 12. Pyrograms of sample KC at 360 °C: pyrogram using the Basic/Bulk-Rock pyrolysis method (a); pyrogram using the MHS pyrolysis (b).

compared to those hydrocarbons generated from sulfur-lean organic facies.

Figs. 11(a–d) and 13(a–d) show the change in sulfur quantities from the thermally immature KC and APM samples and from their corresponding residues after the 300 °C HP experiments. Notice from these two figures the contrast in S2-bound organic sulfur reduction from the immature samples to the samples after the 300 °C HP experiments. This reduction in S2-bound organic sulfur is proportional to the reduction in extracted S2 quantities (last column, Table 1) from immature aliquots to residues after the 300 °C HP experiments. While the Green River Shale sample reports a 39% decrease in extracted S2 (labile kerogen) quantities (180–110 mg/g), the Kimmeridge Clay sample reports an 83% decrease in extracted S2 (labile kerogen) quantities (212–36 mg/g). For the Kimmeridge Clay sample, this is a dramatic percentage of kerogen transformation into hydrocarbons at relatively low levels of thermal stress (VRo-equivalent ~0.58%) and implies that this particular sample of the Kimmeridge Clay formation has a Type II-S character, something that has been previously documented [43]. Moreover, it is anticipated that these thermally "immature" hydrocarbons will likely have a quality that could compromise their proper detection (as hydrocarbons and not as solid kerogen or bitumen) in a HF NMR T1-T2 2-D map.

3.3. 2-Dimensional HF-NMR T1-T2 maps

Fig. 14 shows a generic example of HF NMR T1-T2 2-D map for a shale sample, where different hydrocarbon populations can be seen. The main plot, i.e., the central part of figure with the blue background, is the T1-T2 2-D correlation map, in which the color represents the hydrogen intensity at a given T1 and T2 coordinate. The top plot is 1-D T_2 distribution, which is the projection of the main map onto the T2 axis. It should be noted that T2 distribution in original mudstones is not a measure of pore size distribution due to coexistence of all hydrogen components. Similarly, the left sub-plot is 1-D T1 distribution. Water, oil and solid organics can be identified with the ratios of T1 and T2, although it is a challenging task because of the overlap of solid kerogen and hydroxyl groups signals in Region 3 of the T1-T2 map [44]. The NMR signals in the main plot can be divided into four regions for simple interpretation of the NMR correlation map based on their T1/T2 ratios. Regions (1) and (4) show T1/T2 ratios close to 1 and are interpreted as representing water, and because of its longer T2, water in Region (1) is less bound than water in Region (4). Region (2) has higher T1/T2 ratios and the T2 signals are relatively long indicating that they are from free or light oil. Hydrocarbon molecular mobility changes with T2. Signals on the left (shorter T2) are from the molecules that are less mobile or more restricted, such as heavier or more viscous hydrocarbons, or hydrocarbons present in smaller pores. Signals on the right (longer T2) are from more mobile molecules, such as lighter hydrocarbons or hydrocarbons present in larger pores. Region (3) has much higher T1/T2 ratios and very short T2 signals, so the signals are from solids such as heavy oil, bitumen or organic matter, but the exact origins depend on reservoir formations [16,45] and references therein. The T1/T2 ratios of hydrocarbons are generally greater than 1 but are also viscosity dependent.

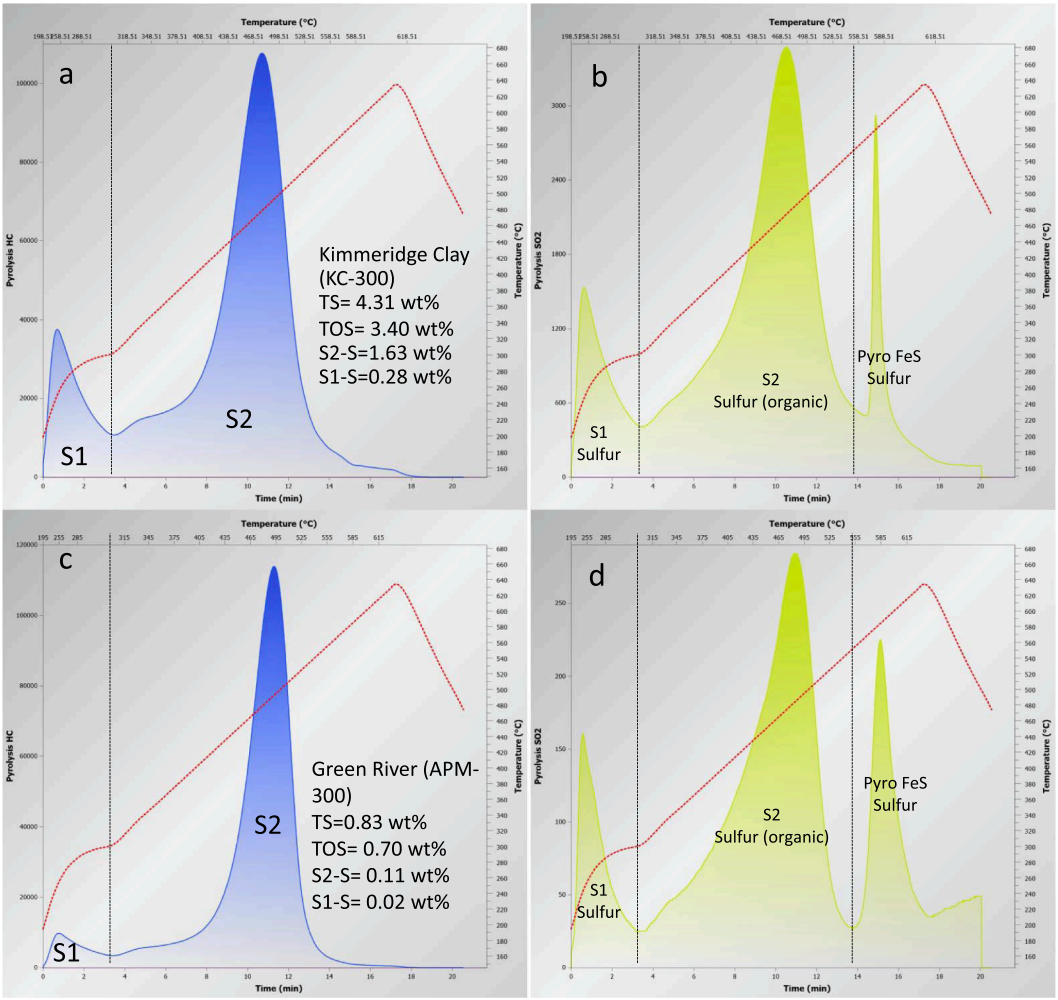

Fig. 13. (a-d) Sulfur quantities (total sulfur, TS, total organic sulfur, TOS, and organic sulfur from labile kerogen, S2, and oil/bitumen, S1) during pyrolysis of the KC (a-b) and APM (c-d) residues following hydrous pyrolysis at 300 °C.

Solid bitumen (and/or heavy hydrocarbons) tend to have a higher T1/T2 ratio. This is confirmed by [46] where T1/T2 ratios of viscous hydrocarbons are much greater than 1 for various heavy crude oils.

To compare with the S2 from pyrolysis, NMR solid signals were acquired using the solid echo pulse and fitted to a combined function of a Gaussian plus an exponential. The amplitude of the components with the shortest time constant, either the Gaussian part or the combined, is used as the measure of the NMR S2 equivalent. An example of how the NMR S2 values were derived is shown in Fig. 15 (a-d) for the APM samples. The same applies to the derivation of the NMR S2 for the KC samples (not shown).

The fraction referred to as "OIL" in Table 1 is thought to contain the total amount of OIP (in mg/g) as detected by modified pyrolysis methods, such as the Reservoir Pyrolysis and Shale Play methods [6,9] and the MHS method (OIL = L1 + L2 + L3 + L4) [42]. The OIL quantities from MHS pyrolysis shown in Table 1 are compared to the total amount of more relaxed hydrocarbon fluids (zones having longer T2 relaxation time) in the T1-T2 map from NMR and to the S1 quantities from Basic/Bulk-Rock pyrolysis analysis. Fig. 16 (a and c) shows the bar graphs of OIL quantities from each of the analysis performed using the three methods. Fig. 16(b and d) shows the quantities of reactive kerogen (S2) detected by the three methods.

The Kimmeridge Clay samples show few differences between the quantities of OIL from NMR and MHS pyrolysis (Fig. 16a), with the differences being between 17 and 76 mg/g). They also show a good agreement between the quantities detected for reactive kerogen (S2) (Fig. 16b), with the differences being as low as 7–8 mg/g and as high as 32 mg/g (Table 1). The Green River Shale samples (Fig. 16c) also show a good agreement between the quantities of OIL from NMR and MHS pyrolysis, with the differences being between 1 and 8 mg/g. The differences between the quantities detected for reactive kerogen (S2) (Fig. 16d) range from 5 mg/g to 48 mg/g (Table 1). It is possible that these differences, for the same type of organic matter at different maturities and between different types of organic matter, may be related to the composition of the hydrocarbon fluid generated from the different types of reactive kerogen [47] and the type of porosity developed upon increased maturity.

The Kimmeridge Clay samples had high hydrocarbon content but produced "less mobile" (i.e., heavy oil/bitumen) hydrocarbons through HP. Significant "movable" oil was produced at 360 °C. This is related to the high sulfur content of the KC-Original kerogen producing heavy oil/bitumen. On the other hand, the APM samples had lower hydrocarbon content (compared to the Kimmeridge Clay samples) but started to produce "movable" oil (more mobile in the molecular dynamics sense) at 330 °C or even lower. This characteristic of the oil could explain the slightly lower bitumen %Ro of 0.12 measured on APM HP at 330 °C (Fig. 10).

Of the eight samples analyzed (2 original plus 6 HP residues), the Kimmeridge Clay sample from the HP experiment at 330 °C (KC-330) shows the highest variation between MHS pyrolysis results and both Basic/Bulk-Rock pyrolysis and NMR values (for both OIL and Reactive kerogen). Fig. 17(a-b) shows the Rock-Eval 7S® pyrograms of both

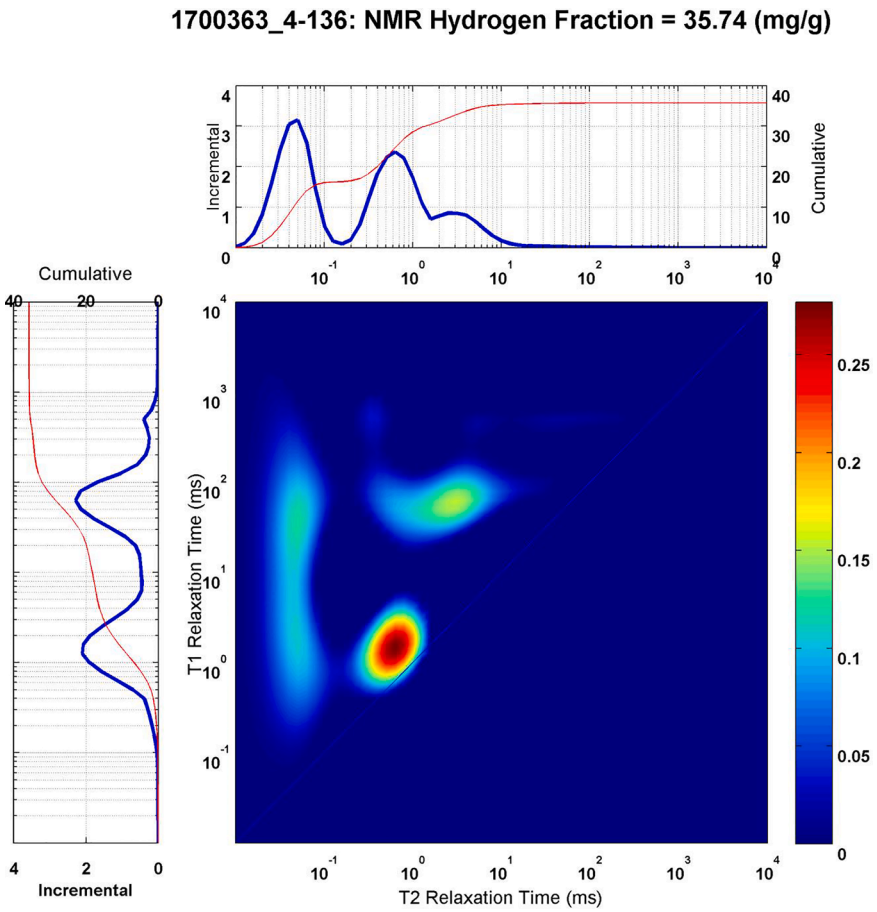

Fig. 14. Generic HF-NMR T1-T2 map showing the four regions (labelled 1 to 4) that correspond to the evolution of different hydrocarbon and water populations.

pyrolysis methods, Basic/Bulk-Rock and MHS, and the NMR T1-T2 map for sample KC-330 (Fig. 17c). The NMR signal, after removal of the rigid solid signal, is only able to clearly differentiate between two hydrocarbon zones, Zones 2 & 3, with a total OIL of 26.8 mg/g. This value is almost half of that measured using the Basic/Bulk-Rock pyrolysis method (S1 = 48.01 mg/g) and almost five-times lower than OIL from MHS pyrolysis (121.04 mg/g). Such a variation in oil quantities detected by the NMR T1-T2 map is likely to be in part due to the quality of hydrocarbons generated (from the sulfur-rich kerogen portion of the S2): low in API gravity, viscous, and sulfur-rich (0.24–0.38 wt% of the whole rock is S1-bound sulfur; Table 2). It is also possible that, in addition to the oil quality, the small pore spaces available to accommodate the newly created hydrocarbons play a large role in the under-detection of mobile hydrocarbons by NMR T1-T2 maps. We investigate this below via Argon ion milled-scanning electron microscopy (AIM-SEM).

3.4. AIM-SEM

Pore size (as seen in the AIM-SEM photos in the KC-Original (Fig. 18a–c) and the KC-330 HP residue (Fig. 19a–c) does not seem to be the cause of this variation. The difference in pore availability and size between the samples is striking: sample KC-Original shows virtually no porosity while, after maturing through hydrous pyrolysis for 72 hrs @ 330 °C, pore space is created throughout the sample, especially in places where organic matter appeared to partly occupy space in the KC-Original sample.

In the case of the Kimmeridge Clay samples, it is possible that the fluid is more viscous than that in the APM samples. Fluid composition affected the NMR measurements, leading to an underestimation of the OIL content. As mentioned earlier, the L1 fraction from MHS pyrolysis has been interpreted to contain the lowest BP hydrocarbons [6,42] and is the fraction with the highest likelihood of being produced. If the volume of liquid hydrocarbons detected in the L1 portion of the MHS pyrolysis is compared with zones 2 and 3 from NMR, the difference for sample KC-330 decreases to < 6 mg/g. This comparison between L1 from MHS pyrolysis and the more relaxed liquid hydrocarbon fractions from NMR (Zones 2, 3 and 4, if present) is shown for all Kimmeridge Clay samples in the bar graphs in Fig. 20. This figure shows that, for the Kimmeridge Clay samples, HF-NMR at room temperature (22 °C) tends to underestimate the volume of producible hydrocarbons. It is only able to differentiate the very lowest BP hydrocarbons from very rigid solids (S2), leaving behind undifferentiated - but potentially producible - liquid hydrocarbons. Such hydrocarbons could be trapped in very small pores in the KC-Original sample, although this is unlikely. This sample is clay-rich and contains small pores with diameters that range from 2 to 10 nm based on N_2 and CO_2 adsorption studies (Birdwell, J.E, U.S. Geological Survey, written comm., November 6, 2020). However, clay-rich inorganic pores tend to be water-wetting surfaces. As a result, it is unlikely that these small pores would store any oil that is generated during hydrous pyrolysis. An alternate explanation is that these liquid hydrocarbons may have a specific chemical composition and fluid properties that mask them from NMR detection at room temperature. Yet, another explanation of the observations seen in the HF-NMR data may, at least in part, be related to the surface area of the two samples. The APM-Original sample has an SSA of ~ 2.8 m^2/g and the KC-Original sample has SSA of ~ 10.9 m^2/g (Birdwell, J.E., U.S. Geological Survey, written comm., November 6, 2020). If the NSO-rich (mainly sulfur) composition of the KC-Original liquid hydrocarbons is high, the hydrocarbons could stick to the clay mineral surfaces. Thus, the NMR analysis should be conducted at higher temperatures for the

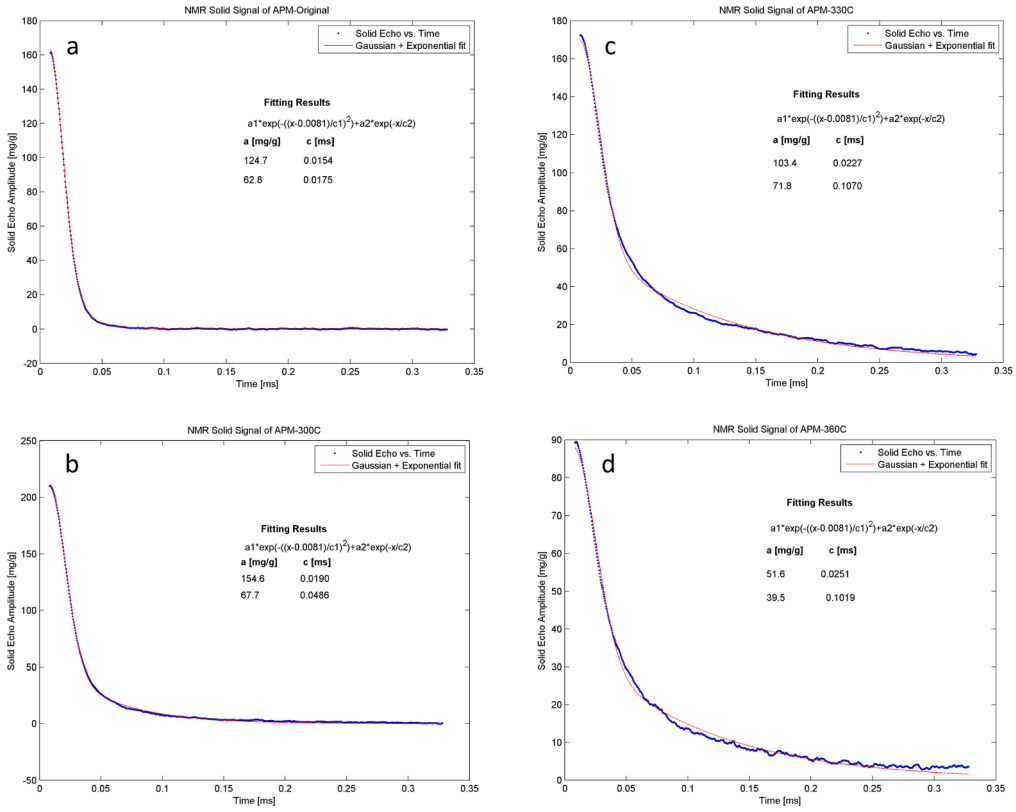

Sample	NMR-S2
APM-Original	187.5
APM-300°C	154.6
APM-330°C	103.4
APM-360°C	51.6

Fig. 15. (a-d) NMR solid signals fitted to a combined function of a Gaussian plus an exponential. The APM-Original (a) shows the Gaussian and exponential functions to have similar time constants; hence, a combined amplitude is used as the measure of NMR-S2. For the other samples at 300 °C (b), 330 °C (c), and 360 °C (d), the amplitude of the Gaussian fit is used as NMR-S2.

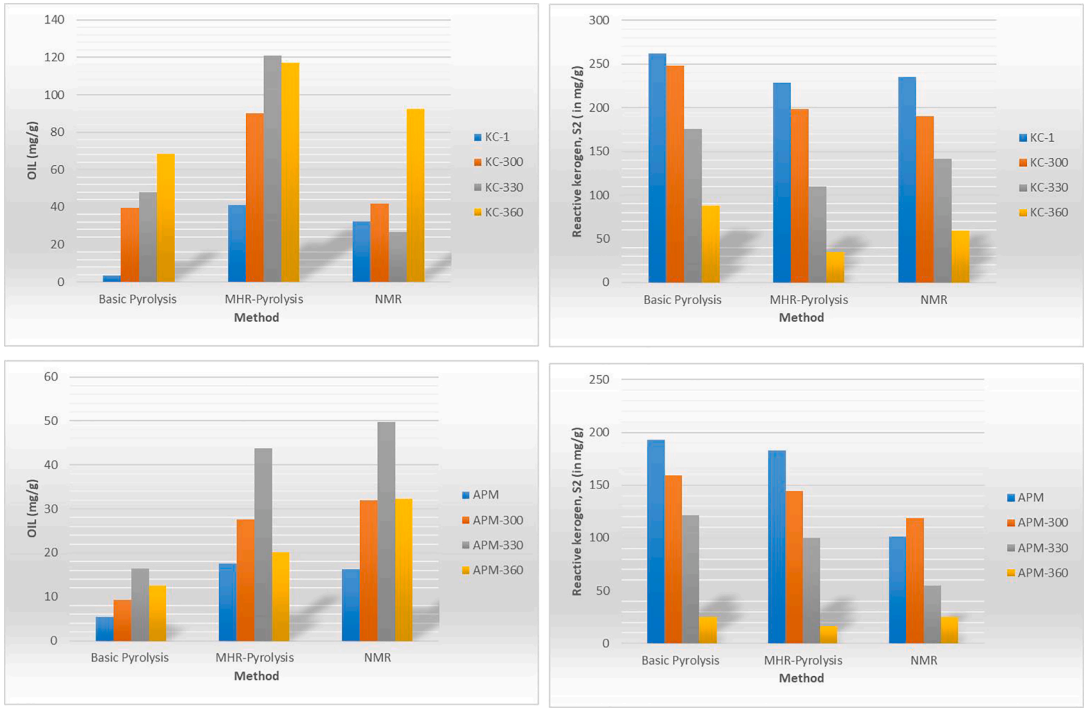

Fig. 16. Comparison of the amount of OIL (L1-L4) and reactive kerogen (S2) of the original samples and their products, obtained by the Basic/Bulk-Rock and MHS pyrolysis methods and the HF-NMR method. (a) and (b) refer to the KC set of samples and (c) and (d) refer to the APM set of samples.

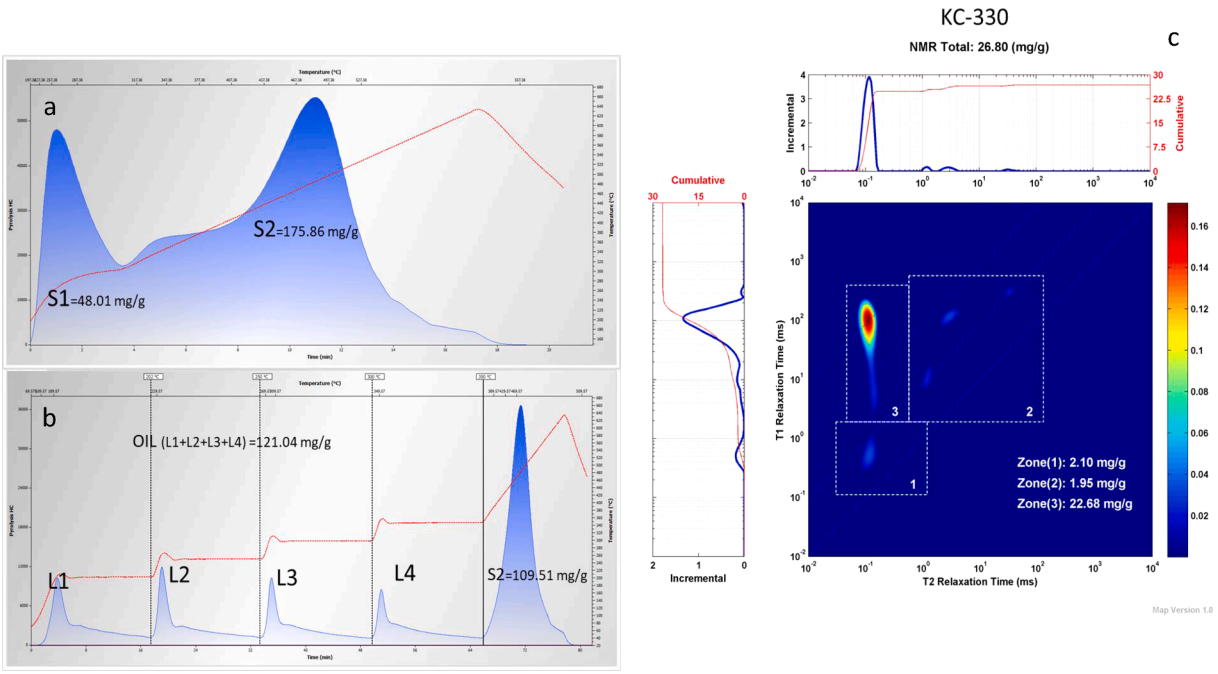

Fig. 17. (a–c) Rock-Eval 7S® pyrograms of Basic/Bulk-Rock pyrolysis (a); MHS pyrolysis (b); and the NMR T1-T2 map (c) for sample KC-330 °C.

Table 2
Total sulfur, total organic sulfur, pyritic sulfur, and organic sulfur associated with the S1 and S2 peaks from pyrolysis of the KC-Original and APM-original samples and their hydrous pyrolysis residues at 300 °C, 330 °C, and 360 °C.

Sample	Total Sulfur (wt. % whole rock)	S1-Sulfur (wt. % whole rock)	S2-Sulfur (wt. % whole rock)	Total Organic Sulfur (wt.% whole rock)	Pyritic Sulfur (wt. % whole rock)
KC-1	5.38	0.24	3.49	4.96	0.36
KC-300	4.31	0.28	1.63	3.4	0.85
KC-330	3.87	0.29	0.89	3.11	0.74
KC-360	3.76	0.38	0.35	2.79	0.96
APM-1	0.89	0.02	0.22	0.72	0.07
APM-300	0.83	0.02	0.11	0.7	0.11
APM-330	0.7	0.02	0.07	0.65	0.02
APM-360	0.69	0.02	0.03	0.55	0.01

undifferentiated liquid hydrocarbons to be detected.

3.5. Effect of NMR temperature

As indicated above, this underestimation of producible liquid hydrocarbons observed in the matured Kimmeridge Clay samples could be related to the temperature at which NMR measurements were taken (room temperature in this case). Since NMR molecular relaxation is heavily impacted by viscosity of the fluid, pore size, and surface affinity (all factors present in LRU plays), producible oil present in very small pores that are probably not seen under AIM-SEM could be mistaken as rigid to semi-rigid solid by NMR because the oil is viscous for NMR standards or has a chemical composition that masks it under room-temperature HF-NMR.

The effect of temperature during NMR measurements was explored [42,48]. Carvajal-Ortiz et al. [42] analyzed samples from the Wolfcamp, Woodford, and Meramec formations in the USA at six different temperatures: 22 °C, 45 °C, 50 °C, 55 °C, 60 °C, and 65 °C. An example for the Wolfcamp Formation in Texas is shown in Fig. 21 (a-c). As temperature increased from 22 °C to 65 °C, the Region 2 hydrocarbons increased slightly from 0.17 to 0.51 mg HC/g, which was attributed to the escape of low BP hydrocarbons from pore spaces. Regions 3 and 4 showed an opposite behavior. Region 4 HCs decreased from 8.99 to 3.89 mg/g while Region 3 hydrocarbons increased from 1.99 to 5.14 mg/g over the same temperature range. At 65 °C, Region 3 is interpreted to contain potentially producible HCs at reservoir temperature. Furthermore, at the same temperature, the solid hydrocarbons in Region 4 appear to move into Region 3. This agrees with the results of [49], who showed that solvated hydrocarbons in Kimmeridge Clay kerogen isolates have similar T1-T2 (T2 ~ 10^{-1} ms, T1 ~ 10 ms) values as those in Region 4 (Figs. 14 and 21 in this study). Thus, the data on kerogen isolates corroborate with the interpretation that some producible hydrocarbons may be present in NMR Region 4 in core samples. The sum of regions L1, L2, and L3 using MHP totals 5.67 mg/g while the sum of regions 2 and 3 from HF-NMR totals 5.65 mg/g, which are identical quantities. Fig. 22 shows the TE-GC of the sample from the Wolfcamp Formation. A noticeable shift in the hydrocarbons that make-up regions L1–L4 in the MHS analysis can be seen with increasing retention time, which is accompanied by a decrease in the relative intensity of the *n*-alkane peaks.

The temperature study data shown in Fig. 21 suggest that, for naturally-generated fluids found in the Meramec Formation (but also in the Wolfcamp and Woodford - data not shown), about 70–80% of the hydrocarbons in the less-relaxed zones of the HF-NMR T1-T2 maps for experiments held at 65 °C (equivalent to Zones 3 & 4 in the APM-Original and KC-Original samples presented herein) have a higher likelihood of being produced than previously thought based on HF-NMR measurements taken at room temperature (22 °C). This, in turn, has an impact on the petrophysical analysis of a LRU formation and on determining the best drilling and completions practices. Ongoing experiments at different temperatures, similar to those presented in Carvajal-Ortiz et al. [42], will decipher whether experimental conditions play a significant role in Kimmeridge Clay analysis and elucidate on the causes of such a variation in the amount of producible oil detected by NMR and MHS pyrolysis methods.

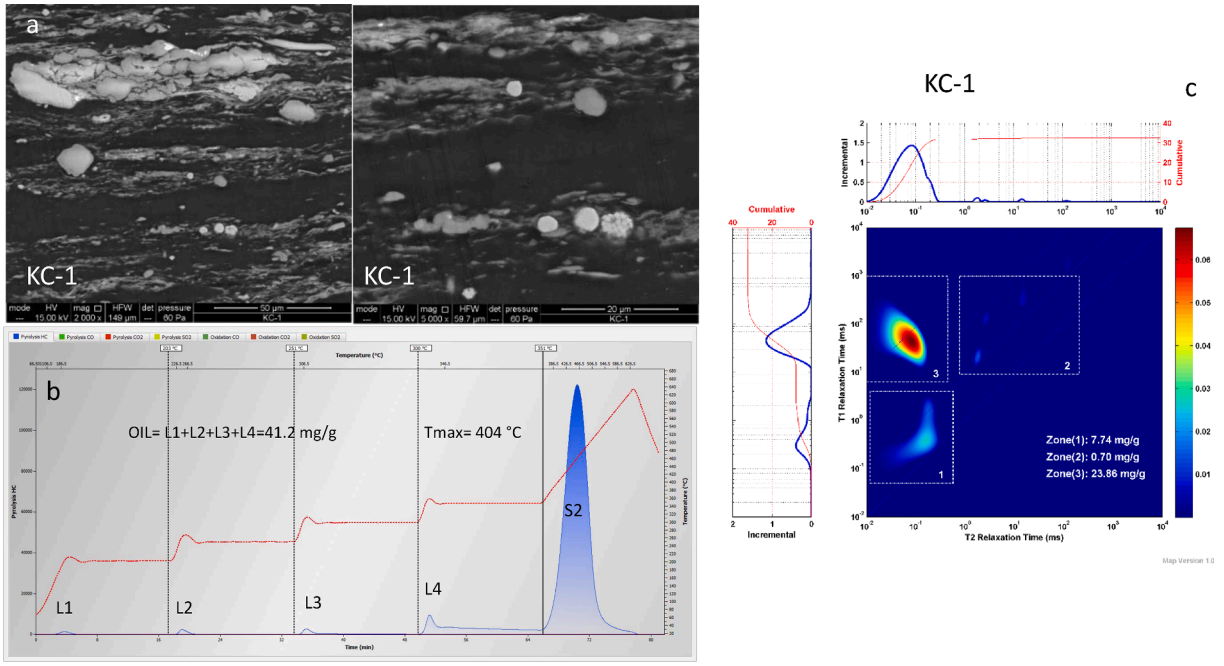

Fig. 18. (a–c) AIM-SEM photos of the original KC-1sample (a), MHS pyrolysis pyrogram (b), and NMR T1-T2 map (c).

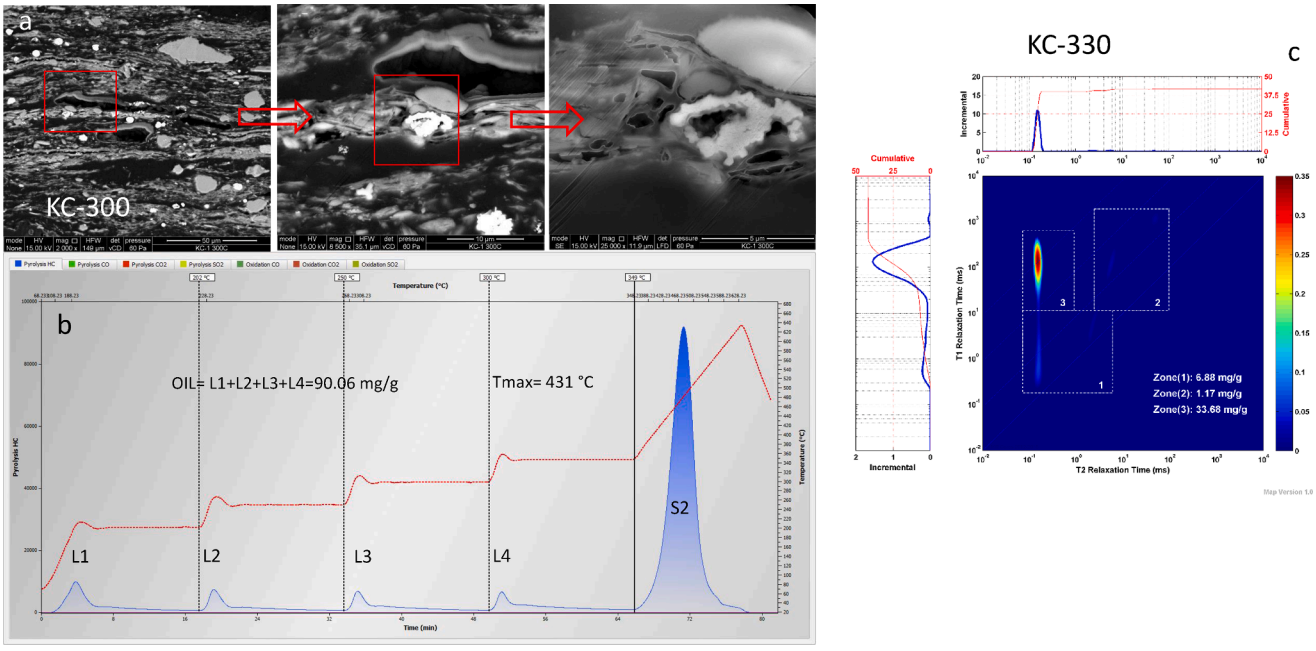

Fig. 19. (a-c) AIM-SEM photos of the KC-330 °C HP residue (a) showing the development and size of pores, MHS pyrolysis pyrogram (b), and NMR T1-T2 map (c).

3.6. The Bakken Shale

Two naturally matured samples, one from the Lower Bakken (%Ro, r = 0.94) and the other from the Upper Bakken (%Ro, r = 0.90) were also subjected to MHS pyrolysis and HF-NMR T1-T2 mapping analysis to determine the agreement between these two methods. The samples were analyzed by NMR at room temperature and the results are shown for the Lower Bakken in Fig. 23(a-b) and for the Upper Bakken in Fig. 24(a-b). Contrary to KC-Original, the agreement between MHS and HF-NMR data in these Bakken Shale samples is very good, with the Lower Bakken sample totaling 11 mg/g by HF-NMR and 12.63 mg/g by MHS pyrolysis. For the Upper Bakken sample, the corresponding totals are 14.4 mg/g and 12.7 mg/g. The above shows that not all liquids-rich shales are expected to behave in a similar fashion. Differences can be seen only when interdisciplinary analytical methods are used, in tandem, to help us better understand the mobility of liquids and, thus, their potential producibility from low-porosity and permeability unconventional formations.

4. Conclusions

The following concluding statements can be made:

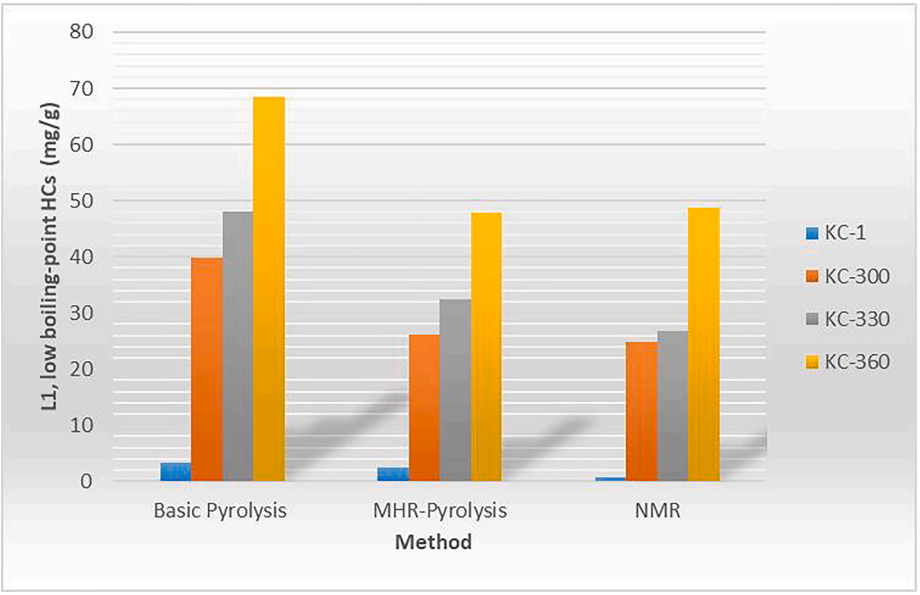

Fig. 20. Comparison between L1 from MHS pyrolysis and the more relaxed liquid hydrocarbon fractions from NMR (Zones 2, 3 and 4) for the KC set of samples.

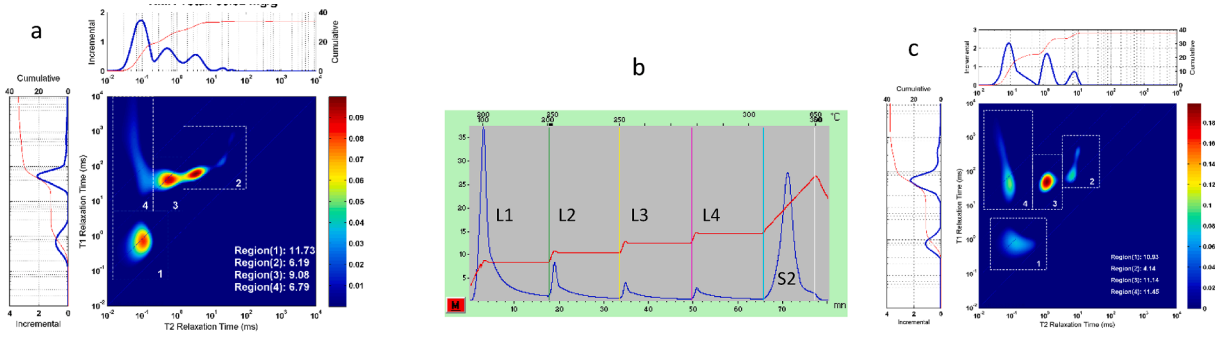

MHS L1=13,32; L2=3.293; L3=1.86; L4=1.25; OIL (L1+L2)=16.61 mg/g; S2=12.40; Tmax=455°C

NMR at 25°C OIL (R3+R4)=16.61; NMR at 45°C OIL=16.60; NMR at 65°C OIL=15.28; NMR at 75°C OIL=14.18 mg/g

Fig. 21. (a–c) Comparison between the HF-NMR measurements of a sample from the Wolfcamp Formation in west Texas taken at 22 °C (a), at 65 °C (b), and its MHS measurements (c). The HF-NMR values from regions 2 + 3 at 45 °C and at 75 °C are also shown for comparison.

- Current resource assessments using Basic/Bulk-Rock pyrolysis on as-received material and on solvent-extracted material tend to either underestimate or overestimate the OIP present in LRU plays. The need for modified pyrolysis methods, such as MHS, combined with HF-NMR, is required for a complete characterization of the true OIP.
- Organic petrography showed that the Green River Shale original sample is rich in strongly fluorescing amorphous organic matter, thin solid bitumen lamellae, telalginite, and small amounts of inertinite. Newly formed solid bitumen having different shapes and showing mobility is present at HP residues above 340 °C. This solid bitumen is converted to coke with anisotropic medium-grained mosaic texture at 350 to 360 °C, suggesting that the carbon is of the graphitizing type. The Kimmeridge Clay Original sample also contains solid bitumen and fluorescing amorphous matrix, along with telalginite and inertinite. A continuous matrix of solid bitumen entraining minerals and refractory inertinite is seen in the HP residues.
- Reflectance of the solid bitumen (BRo) in both samples increases with HP temperature and merges at 360 °C. Sample APM-Original has lower BRo than sample KC-Original over the same HP temperature range. The most noticeable BRo increase (jump) in APM is noted between 330 °C and 350 °C whereas KC exhibits a more gradual increase in BRo. As expected, visible fluorescence color and intensity diminish at 300 °C and completely disappear thereafter.
- HF-NMR Zones 2 + 3 and MHS pyrolysis (L1 fraction) are in good agreement in terms of HC quantities, when HF-NMR measurements are taken at room temperature (22 °C). L1 contains the lowest BP hydrocarbon fraction, which is easily producible from the chemical make-up point of view but is not the only producible fraction found in LRU plays.
- For the Kimmeridge Clay sample, HF-NMR at room temperature (22 °C) tends to underestimate the volume of producible hydrocarbons. It is only able to differentiate the very lowest BP hydrocarbons leaving behind potentially producible liquid hydrocarbons. Discrepancies may be due to the type of porosity (e.g., liquid hydrocarbons trapped in very small pores) or to the chemical composition of the liquid hydrocarbons (likely to be viscous and relatively high in sulfur due to early generation from Type II-S fraction of the oil-prone kerogen), which makes them undetectable by HF-NMR at room temperature. The discrepancies may also be related to the larger surface area of the KC-Original clays, which tend to adsorb the S-rich NSO (heavier) compounds that are more abundant in the KC-Original sample.

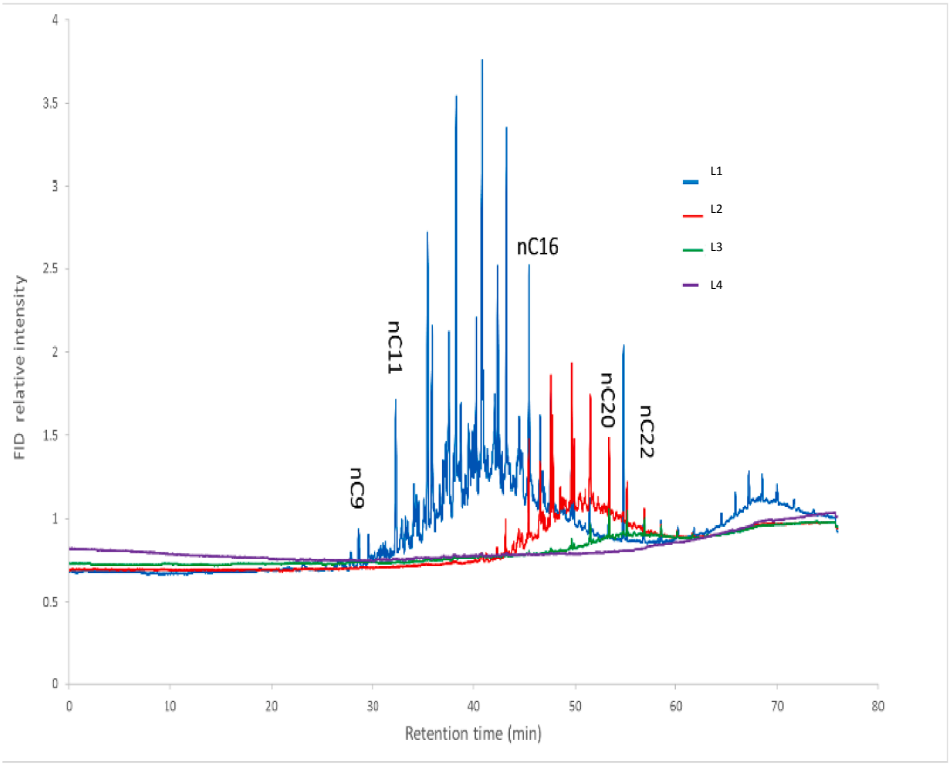

Fig. 22. Thermal Extraction Gas Chromatogram (TE-GC) of the sample from the Wolfcamp Formation. Note the shift in the hydrocarbons that make-up regions L1 to L4 in the MHS analysis and decrease in their relative intensity with increasing retention time.

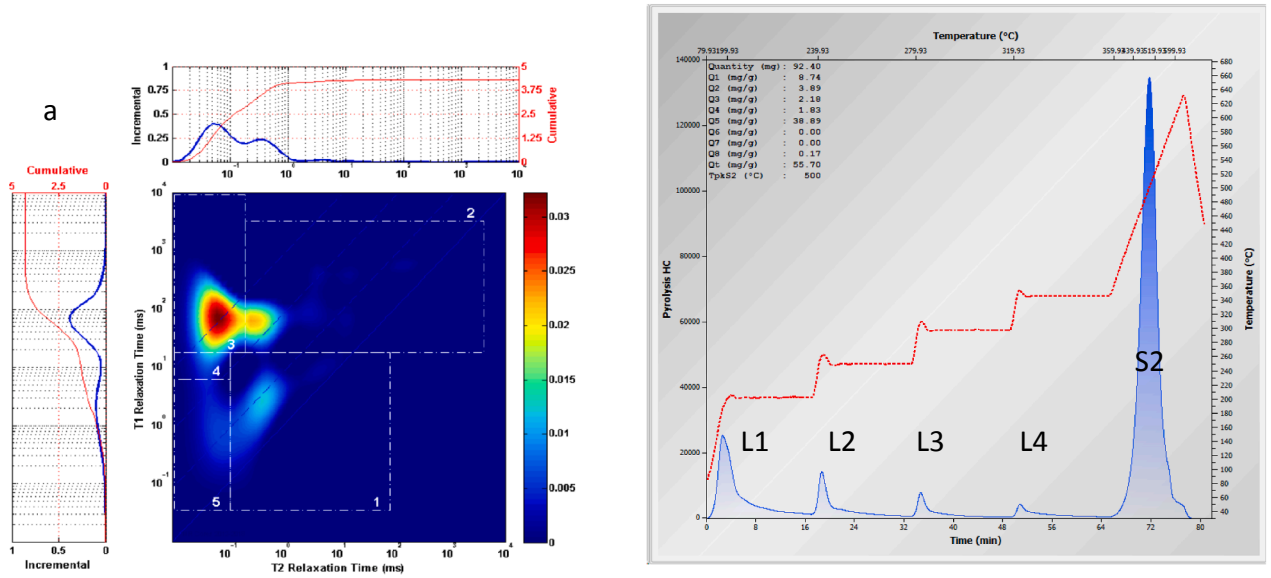

Fraction	NMR	MHS
Oil	11 mg/g	12.63 mg/g
Solid	32.9 mg/g	38.9 mg/g

Fig. 23. (a-b) HF-NMR T1-T2 map of the Lower Bakken at room temperature (a) and the MHS pyrogram (b).

- On the other hand, H-NMR and MHS tests conducted on Lower and Upper Bakken Shale samples containing marine Type II kerogen at 22 °C showed a much closer agreement between the amounts of oil calculated by the two methods. This suggests that each LRU formation should be treated individually and by following an integrated analytical approach.

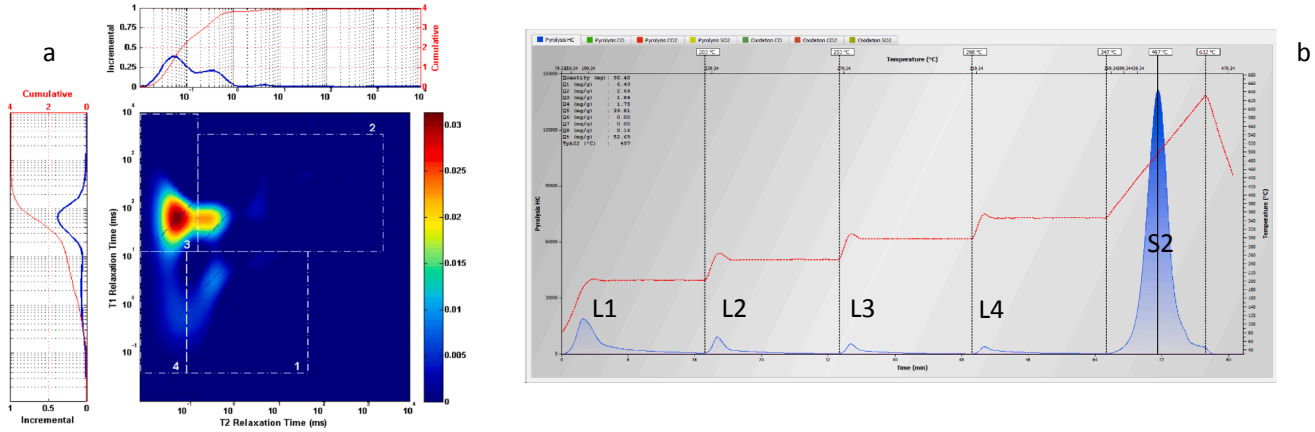

Fraction	NMR	MHS
Oil	14.4 mg/g	12.7 mg/g
Solid	32.2 mg/g	39.8 mg/g

Fig. 24. (a-b) HF-NMR T1-T2 map of the Upper Bakken at room temperature (a) and the MHS pyrogram (b).

- HF-NMR at room temperature appears to underestimate the amount of OIP for certain types of organic-rich LRU resources. Therefore, NMR analysis at higher temperatures is required to determine whether any of the less-relaxed hydrocarbons in Zones 3 & 4 could be mobilized and produced, thus providing a better correlation between HF-NMR and MHS pyrolysis data. HF-NMR experiments conducted at 65 °C showed that almost 70–80% of the hydrocarbons in the less relaxed zones of the T1-T2 maps (equivalent to Zones 3 & 4) could be producible. This is a considerably higher percentage than normally anticipated and has important implications regarding drilling and completion strategies.
- The complexity in constituent components of liquids-rich shales has made it necessary to employ a combination of analytical methods that help us better understand the process of liquids mobility and potential producibility from such formations.

CRediT authorship contribution statement

Thomas Gentzis: Conceptualization, Methodology, Validation, Investigation, Resources, Writing - original draft, Writing - review & editing, Visualization. **Humberto Carvajal-Ortiz:** Conceptualization, Methodology, Validation, Investigation, Resources, Writing - original draft, Writing - review & editing, Visualization. **Z. Harry Xie:** Conceptualization, Methodology, Validation, Investigation, Resources, Writing - original draft, Writing - review & editing, Visualization. **Paul C. Hackley:** Methodology, Validation, Investigation, Resources, Writing - review & editing, Visualization. **Hallie Fowler:** Investigation.

Declaration of Competing Interest

The authors declare that they have no known competing financial interests or personal relationships that could have appeared to influence the work reported in this paper.

Acknowledgments

Both original samples were collected by Dr. Michael D. Lewan and aliquots were provided by the U.S. Geological Survey Petroleum Geochemistry Research Laboratory in Denver, CO. We also thank Dr. Justin E. Birdwell for reviewing an earlier draft of the manuscript and providing valuable comments and suggestions, which improved the quality of the manuscript. Finally, we would like to express our gratitude to the three anonymous reviewers for their constructive comments and to Principal Editor Dr. Eric Suuberg for handling our manuscript in a professional manner. Use of trade, product, or firm names is for descriptive purposes only and does not imply endorsement by the U.S. Government.

References

[1] Jarvie, D.M., 2012. Shale resource systems for oil and gas: part 2—shale–oil resource systems. In: Breyer, J.A. (Ed.), Shale Reservoirs—Giant Resources for the 21st Century. AAPG Memoir 97, pp. 89–119.
[2] Jarvie DM. Components and processes affecting producibility and commerciality of shale resource systems. Geologica Acta 2014;12:307–25.
[3] Espitalié J, Laporte JL, Madec M, Marquis F, Leplat P, Paulet J. Methode rapide de caracterisation des roches-meres, de leur potentiel petrolier et de leur degre d'evolution. Rev Inst Fr Petr 1977;32:23–43.
[4] Espitalié J, Deroo G, Marquis F. Pyrolysis and its applications. Part II: Revue de l'Institut Francais du Petrol 1985;40:755–84.
[5] Peters KE. Guidelines for evaluating petroleum source rock using programmed pyrolysis. AAPG Bull 1986;70:318–29.
[6] Romero-Sarmiento MF, Pillot D, Letort G, Lamoureaux-Var V, Beaumont V, Huc AY, et al. New Rock-Eval method of unconventional shale reservoir systems. *Review Institut Français du Pétrole Energ.* Nouv 2015;71:1–9. https://www.researchgate.net/publication/274070444_New_Rock-Eval_Method_for_Characterization_of_Unconventional_Shale_Resource_Systems.
[7] Carvajal-Ortiz H, Gentzis T. Geochemical screening of source rocks and reservoirs: The importance of using the proper analytical program. Int J Coal Geol 2018;190:56–69.
[8] Abrams MA, Gong C, Garnier C, Sephton MA. A new thermal extraction protocol to evaluate liquid rich unconventional oil in place and in-situ fluid chemistry. Mar Pet Geol 2017;88:659–75.
[9] Trabelsi K, Espitalié J, Huc AY. Characterization of extra heavy oils and tar deposits by modified pyrolysis methods. In: Proceedings of the "Heavy Oil Technologies in a Wider Europe" Thermie EC Symposium; 1994. p. 30–40.
[10] Collins D, Lapierre S. Integrating solvent extraction with standard pyrolysis to better quantify thermal maturity and hydrocarbon content in the oil window. Unconvent Resour Technol Conf (URTeC) 2014. https://doi.org/10.15530/urtec-2014-1922397.
[11] Raji M, Gröcke DR, Greenwell C, Cornford C. Pyrolysis, porosity, and productivity in unconventional mudstone reservoirs: free and adsorbed oil. Unconvent Resour Technol Conf (URTeC) 2015. https://doi.org/10.15530/urtec-2015-2172996.
[12] Dang TS, Sondergeld CH, Rai CS. Reducing ambiguity in source rock analyses. Unconvent Resour Technol Conf (URTeC) 2016. https://doi.org/10.15530/urtec-2016-2461388.
[13] Piedrahita, J. and Aguilera, R., 2017. Estimating Oil Saturation Index OSI from NMR Logging and Comparison with Rock-Eval Pyrolysis Measurements in a Shale Oil Reservoir, SPE Unconventional Resources Conference. Society of Petroleum Engineers. SPE-185073-MS.
[14] Romero-Sarmiento MF, Euzen T, Rolais S, Juang C, Littke R. Artificial thermal maturation of source rocks at different thermal maturity levels: applications to the Triassic and Doig formations in the western Canada sedimentary basin. Org Geochem 2016;97:148–62.

[15] Nowaczewski, V.S., Barton, J., Lagunes, B., Tang, A., Lewan, M.D. 2019. Low-temperature hydrous pyrolysis (LTHP) on oil-field core-samples for estimating original in-place retained oil in mature source rocks and tight-oil reservoirs. AAPG Datapages/Search and Discovery Article #90349, AAPG Hedberg Conference, The Evolution of Petroleum Systems Analysis: Changing of the Guard from Late Mature Experts to Peak Generating Staff, Houston, Texas, March 4-6.
[16] Washburn KE, Birdwell JE. Updated methodology for low field nuclear magnetic resonance characterization of shales. J Magn Reson 2013;233:17–28.
[17] Washburn KE, Anderssen E, Seymour JD, Codd S, Birdwell JE, Vogt SJ, et al. Simultaneous Gaussian and exponential inversion for improved analysis of shales by NMR relaxometry. J Magn Reson 2015;250:7–16.
[18] Birdwell JE, Washburn KE. Multivariate analysis relating oil shale geochemical properties to relaxometry. Energy Fuels 2015;29:2234–43.
[19] Birdwell JE, Washburn KE. Rapid analysis of kerogen hydrogen-to-carbon ratios in shale and mudrocks by laser-induced breakdown spectroscopy. Energy Fuels 2015; 29:6999–7004.
[20] Li J, Jiang C, Wang M, Lu S, Chen Z, Chen Z, et al. Adsorbed and free hydrocarbons in unconventional shale reservoir: a new insight from NMR T1–T2 maps. Mar Pet Geol 2020;116:104311.
[21] Song Y-Q, Venkataramanan L, Hürlimann MD, Flaum M, Frulla P, Straley C. T1–T2 spectra obtained using a fast two-dimensional Laplace inversion. J Magn Reson 2002;154:261–8.
[22] Lewan MD, Spiro B, Illich H, Raiswell R, Mackenzie AS, Durand B, et al. Evaluation of petroleum generation by Hydrous Pyrolysis experimentation. Philos Trans R Soc Lond 1985;315:123–34.
[23] Fowler MG, Gentzis T, Goodarzi F, Foscolos AE. The hydrocarbon potential of some Tertiary lignites from northern Greece as determined using pyrolysis and organic petrological techniques. Org Geochem 1991;17:805–26.
[24] Hackley PC, Lewan M. Understanding and distinguishing reflectance measurements of solid bitumen and vitrinite using hydrous pyrolysis: Implications to petroleum assessment. AAPG Bull 2018;102:1119–40.
[25] Washburn KE, Birdwell JE, Howard JJ. Real-time specific surface area measurements via laser-induced breakdown spectroscopy. Energy Fuels 2017;31: 458–63.
[26] Lamoureux-Var, V., Espitalié, J., Pillot, D., Bouton, N., Garcia, B., Antonas, R., Aboussou1, A., Wattripont, A., Ravelojaona, H., Noirez, S., Beaumont, V., 2019. ROCK-EVAL 7S: Technology and Performance. 29th International Meeting on Organic Geochemistry. IMOG), Gothenburg, Sweden.
[27] Aboussou A, Lamoureux-Var V, Wagner T, Pillot D, Kowalewski I, Garcia MC, et al. Pyritic sulphur and organic sulphur quantification in organic rich sediments using Rock-Eval 7S. In: Conference Proceedings, First EAGE/IFPEN Conference on Sulfur Risk Management in Exploration and Production; 2018. https://doi.org/10.3997/2214-4609.201801129.
[28] Wattripont, A., Bouton, N., Espitalie, J., Antonas, R., Constantinou, G., 2018. Rock-eval sulfur & GEOWORKS software. In: Conference Proceedings, First EAGE/IFPEN Conference on Sulfur Risk Management in Exploration and Production. https://doi.org/10.3997/2214-4609.201802756. Sep 2018, cp-565-00003.
[29] ASTM, 2014a, D2797 Standard practice for preparing coal samples for microscopical analysis by reflected light. Annual book of ASTM standards: petroleum products, lubricants, and fossil fuels; gaseous fuels; coal and coke, sec. 5, v. 05.06. West Conshohocken, PA: ASTM International.
[30] ASTM, 2014b, D7708 Standard test method for microscopical determination of the reflectance of vitrinite dispersed in sedimentary rocks. Annual book of ASTM standards: petroleum products, lubricants, and fossil fuels; gaseous fuels; coal and coke, sec. 5, v. 5.06, West Conshohocken, PA: ASTM International.
[31] Hackley PC, Araujo CV, Borrego AG, Bouzinos A, Cardott BJ, Cook AC, et al. Standardization of reflectance measurements in dispersed organic matter: results of an exercise to improve interlaboratory agreement. Mar Pet Geol 2015;59:22–34.
[32] Horsfield B, Curry DJ, Bohacs K, Littke R, Rullkötter J, Schenk HJ, et al. Organic geochemistry of freshwater and alkaline lacustrine sediments in the Green River Formation of the Washakie Basin, Wyoming, USA. Org Geochem 1994;22:415–40.
[33] Schieber, J., 2007. Benthic microbial mats as an oil shale component: Green River Formation (Eocene) of Wyoming and Utah, in: Schieber, J., Bose, P.K., Eriksson, P. G., Banerjee, S., Sarkar, S., Altermann, W., Catuneau, O. (Eds.), Atlas of microbial mat features preserved within the clastic rock record. Elsevier Atlases in Geosciences 2, 225-232.
[34] Bertrand P, Lallier-Verges E, Boussafir M. Enhancement of accumulation and anoxic degradation of organic matter controlled by cyclic productivity: a model. Org Geochem 1993;22:511–20.
[35] Fishman NS, Hackley PC, Lowers HA, Hill RJ, Egenhoff SO, Eberl DD, et al. The nature of porosity in organic-rich mudstones of the Upper Jurassic Kimmeridge Clay Formation, North Sea, offshore United Kingdom. Int J Coal Geol 2012;103: 32–50.
[36] Hackley PC, Valentine BJ, Hatcherian JJ. On the petrographic distinction of bituminite from solid bitumen in immature to early mature source rocks. Int J Coal Geol 2018;196:232–45.
[37] Macquaker JHS, Gawthorpe RL. Mudstone lithofacies in the Kimmeridge Clay Formation, Wessex Basin, southern England: implications for the origin and controls on the distribution of mudstones. J Sediment Petrol 1993;63:1129–43.
[38] Scotchman IC. Kerogen facies and maturity of the Kimmeridge Clay Formation in southern and eastern England. Mar Pet Geol 1991;8:278–95.
[39] Baskin DK, Peters KE. Early characteristics of a sulfur-rich Monterey kerogen. AAPG Bull 1992;76:1–13.
[40] Marsh H, Diez MA. Mesophase of Graphitizable Carbons. In: Shibaev VP, Lam L, editors. Liquid Crystalline and Mesomorphic Polymers. New York, NY: Springer; 1994. https://doi.org/10.1007/978-1-4613-8333-8_7.
[41] Oberlin A. Carbonization and graphitization. Carbon 1984;22:521–41. https://doi.org/10.1016/0008-6223(84)90086-1.
[42] Carvajal-Ortiz H, Xie H, Gentzis T, Kunkel L, Grinstead C. HF-NMR meets geochemical screening: an integrated approach to examine producibility in organic-rich source and reservoir rocks. 15th Latin American Congress on Organic Geochemistry (ALAGO). 2018.
[43] Boussafir M, Lallier-Vergès E. Accumulation of organic matter in the Kimmeridge Clay Formation (KCF): An update fossilisation model for marine petroleum source-rocks. Mar Pet Geol 1997;14:75–83.
[44] Fleury M, Romero-Sarmiento M. Characterization of shales using T1–T2 NMR maps. J Petrol Sci Eng 2016;137:55–62.
[45] Khatibi S, Ostadhassan M, Xie ZH, Gentzis T, Bubach B, Gan Z, et al. NMR relaxometry a new approach to detect geochemical properties of organic matter in tight shales. Fuel 2019;235:167–77.
[46] Singer PM, Chen Z, Alemany LB, Hirasaki GJ, Zhu K, Xie ZH, et al. Interpretation of NMR relaxation in bitumen and organic-rich shale using polymerheptane mixes. Energy Fuels 2018;32(2):1534–49.
[47] Jin JM, Kim S, Birdwell JE. Molecular characterization and comparison of shale oils generated by different pyrolysis methods. Energy Fuels 2012;26:1054–62.
[48] Romero-Sarmiento MF, Ramiro-Martinez S, Berthe G, Fleury M, Littke R. Geochemical and petrophysical source rock characterization of the Vaca Muerta Formation: implications for unconventional resource estimations. Int J Coal Geol 2017;184:27–41.
[49] Singer PM, Chen Z, Wang X, Hirasaki GJ. Diffusive coupling in heptane-saturated kerogen isolates evidenced by NMR T1–T2 and T2–T2 maps. Fuel 2020;280: 118626.